Plasma Processes and Polymers

Fluid Modeling of the Conversion of Methane into Higher Hydrocarbons in an Atmospheric Pressure Dielectric Barrier Discharge

Christophe De Bie, Bert Verheyde, Tom Martens, Jan van Dijk, Sabine Paulussen, Annemie Bogaerts*

A one-dimensional fluid model for a dielectric barrier discharge in methane, used as a chemical reactor for gas conversion, is developed. The model describes the gas phase chemistry governing the conversion process of methane to higher hydrocarbons. The spatially averaged densities of the various plasma species as a function of time are discussed. Besides, the conversion of methane and the yields of the reaction products as a function of the residence time in the reactor are shown and compared with experimental data. Higher hydrocarbons (C_2H_y and C_3H_y) and hydrogen gas are typically found to be important reaction products. Furthermore, the main underlying reaction pathways are determined.

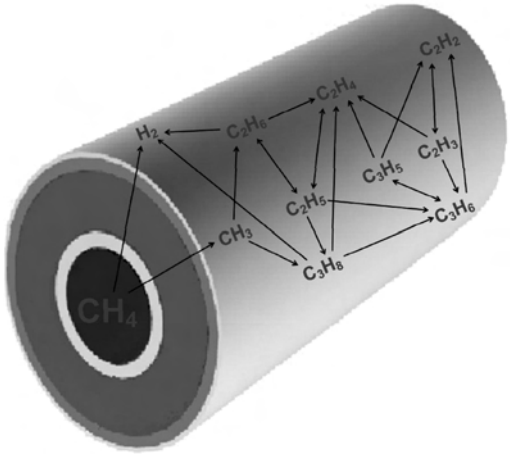

Introduction

The world primary energy demand will increase by 1.6% per year on average between now and 2030 and fossil fuels will account for 80% of the world's primary energy mix in 2030, which means only a slight decrease compared to today.[1] Oil will remain the dominant fuel, even though its share will decrease from 34% today to 30% in 2030. The global demand for oil will rise by 1% per year on average. The demand for natural gas will grow more quickly, by 1.8% per year and its share will increase slightly to 22%. The demand for coal will rise the most with an increase by 2% every year on average and as a result its share will rise to 29% in 2030.[1]

The worldwide non-renewable energy resources such as fossil fuels are, however, finite and it becomes more difficult to recover them. On the basis of the estimated recoverable resources for fossil fuels and the current tendency concerning the growing demand for energy, one predicts that there is enough oil to supply the world for over 60 years, while natural gas and coal reserves should last 130 years and 2000 years, respectively.[1] Globally, these fossil fuel resources may still seem plentiful, but there can be no guarantee that they will be exploited fast enough to meet the level of demand.

The availability of energy resources is, however, of paramount importance to the society. Access to reliable, affordable commercial energy provides the basis for heat, light, mobility, communications and agricultural and industrial capacity in modern society and in this way energy stipulates the degree of civilization.[2]

C. De Bie, T. Martens, A. Bogaerts
Research Group PLASMANT, Department of Chemistry, University of Antwerp, Universiteitsplein 1, 2610 Wilrijk-Antwerpen, Belgium
E-mail: annemie.bogaerts@ua.ac.be
B. Verheyde, S. Paulussen
VITO NV, Vlaamse Instelling voor Technologisch Onderzoek, Plasma Technology, Boeretang 200, 2400 Mol, Belgium
J. van Dijk
Department of Applied Physics, Eindhoven University of Technology, Den Dolech 2, Postbus 513, 5600 MB Eindhoven, The Netherlands

DOI: 10.1002/ppap.201100027

Besides this, the recovery, production, and use of fossil fuels is accompanied by the emission of greenhouse gases and contributes in this way to global warming. Climate change due to anthropogenic greenhouse gas emission is a growing concern for the global society. The global warming observed during the last 50 years is largely due to human activity and the CO_2 emissions that arise when fossil fuels are burnt.[3]

Socially, environmentally and economically a growing demand is being imposed for sustainability in the way energy resources are utilized. A global sustainable energy strategy that meets the increasing demand is based on an improvement of the energy efficiency of the current technologies and a more intensifying diversification of the energy resources with a huge preference for lower carbon resources.

In a world in which fossil fuels make the day, natural gas has the most significant growth potential and so it becomes more and more an interesting alternative for crude oil as feedstock for the chemical industry. Natural gas is currently the third most used energy resource in the world after crude oil and coal,[1] but the lifetime of gas resources is much longer than for oil and its lower carbon content makes natural gas a more environmentally friendly energy source than crude oil and coal. The principal component of natural gas is methane.

Methane, which is an important greenhouse gas, is currently mainly being used for home and industrial heating and for the generation of electrical power. On the other hand, methane is a greatly underutilized resource for the production of chemicals and liquid fuels, mainly because it is one of the most stable molecules.[4] Direct synthesis of hydrocarbons starting from methane is not yet feasible and the conventional indirect methods for partial and total oxidation of methane have poor yields and require high amounts of energy.[5] The utilization of natural gas as a chemical resource is currently limited to the production of synthesis gas (i.e., syngas: $H_2 + CO$) by steam reforming, which is a highly energy-intensive process.[6]

A sustainable process for the conversion of these abundant methane reserves into more value-added chemicals and fuels is therefore renowned as a challenge for the 21st century.[4] More in particular, the development of a process for the direct synthesis of higher hydrocarbons and oxygenates from methane in an energy-efficient way towards economy and environment would offer significant benefits, because this will circumvent the very expensive syngas step.[7]

The major difficulty for the direct conversion of methane is the activation of the stable C–H bond. Conventional methods, using a high temperature and a noble catalyst, require high amounts of energy and lack selectivity.[6] Atmospheric pressure non-thermal low-temperature plasmas can offer here a distinct advantage, because they enable in a unique way gas phase reactions at ambient conditions. Different plasma activation mechanisms cause vibrational and electronic excitation, and ionization and dissociation of species, and in this way gas conversion processes are induced. A dielectric barrier discharge (DBD) has this property because, unlike other non-equilibrium discharges, it can be operated at elevated (0.1–10 bar) pressure, while remaining at ambient temperature.

A DBD is generated between two electrodes of which at least one is covered with a dielectric material made of glass, quartz, alumina, etc. The gap between the two electrodes is typically a few millimeters. An ac voltage with an amplitude from 1 to 100 kV and a frequency of a few Hz to MHz is usually applied to this kind of discharges. Detailed information on the history and the characteristics of a DBD can be found in literature.[8–13] DBDs can be used in a wide variety of applications.[13–16] Reactive species in the discharge (free radicals, electrons, ...) will cause decomposition of the molecules initially present in the gas mixture and afterwards recombination will lead to the formation of value-added and/or less hazardous end products.[13,17–20]

Nowadays a lot of research is carried out on the use of a DBD for the conversion of the greenhouse gases CH_4 and CO_2 to higher hydrocarbons, oxygenates, and syngas.[5,6,21–38] Experimental results on the conversion in a pure methane plasma show that the typical end products are H_2 and higher hydrocarbons, mostly C_2H_6 and in a lower content C_3H_8, C_2H_4, and C_2H_2.[5,29,36] However, there are still a lot of issues open for discussion. More specifically, with respect to the energy efficiency a lot of research work still has to be performed to come to a sustainable industrial process. A better insight into the huge underlying plasma chemistry acting in the methane conversion process would therefore be of great value. Fluid modeling can offer the experimentalist the necessary information to understand the role of the different species in the immensity of chemical reactions taking place in the discharge gap.

Modeling results on gas phase physics and chemistry in different kind of methane containing discharges have been investigated extensively during the past thirty years.[39–57] A minority of them concerns the modeling of the plasma as a gas conversion reactor.[45,48,51,53,56] Up to now these numerical studies mostly concerned zero-dimensional simulations largely based on specific empirical input so that semi-empirical simulations were obtained, which are only valid for the experimental set-up under study. Only Yang[48] used a more generic method to describe the gas conversion in a pure methane plasma, which can be generally used for this kind of gas discharges. However, in this paper a 0D model is used, the plasma chemistry presented is limited and the presented results are rather preliminary.

The aim of our research is to examine the possibility of using plasma-enhanced catalysis for the conversion of CH_4 in the presence of oxygen or carbon dioxide into higher

DOI: 10.1002/ppap.201100027

oxygenates and syngas. More specifically, our goal is to determine whether these gas conversion processes in a DBD may occur in an energy-efficient way and thus whether a process can be developed that is competitive with currently existing or emerging technologies. In order to optimize such a process to become competitive, it is essential to understand the underlying plasma chemistry. This is certainly the case if the purpose is to improve the selectivity of the conversion process in order to obtain a higher yield for one or more of the reaction products by using a heterogeneous catalyst acting on one or more of the underlying gas-phase reactions.

In order to achieve our goal, we started by developing a 1D fluid model to describe in detail the plasma chemistry in an atmospheric pressure DBD in pure methane. In this paper, we present our most important results on the conversion of CH_4 into higher hydrocarbons. First of all, the spatially averaged densities of the various plasma species as a function of time will be discussed. Furthermore, the conversion of CH_4, and the yields and selectivities of the reaction products will be shown. Finally, the main underlying reaction pathways for the conversion of CH_4 into higher hydrocarbons will be pointed out.

Description of the Model

The model employed in this study is a one-dimensional fluid model called Plasimo's MD2D. Originally MD2D was developed to describe the behavior of microdischarges in display technology, such as plasma addressed liquid crystal (PALC) and plasma display panel (PDP) technology.[58–61] Later the model was transformed and extended by Brok et al.[62] and incorporated into Plasimo. In this way the model has previously been used for investigating the breakdown phenomena in compact fluorescent lamps,[62–64] the discharge characteristics of the plasma needle,[65] the behavior of DBDs at low pressure,[66] and the characteristics of DBDs used as ionization source in analytical spectrochemistry.[67–69]

The Fluid Model

Analogous to other fluid models used for the description of low temperature plasmas,[70–74] our fluid model is based on a set of balance equations derived from the Boltzmann transport equation. The first equation is the particle continuity equation which describes the continuity of each type of species p incorporated in the model in terms of its density n_p, flux $\vec{\Gamma}_p$ and source S_p as a function of time and space:

$$\frac{\partial n_p}{\partial t} + \vec{\nabla} \cdot \vec{\Gamma}_p = S_p \tag{1}$$

The source term S_p is obtained by considering the volume reactions in which species p are produced or lost. The second equation is the drift-diffusion equation which describes the flux $\vec{\Gamma}_p$ of each type of species p by means of the summation of a drift component (only for the charged species), driven by the electric field $\vec{E}$, and a diffusion component, caused by the gradient of the density:

$$\vec{\Gamma}_p = \pm \mu_p \vec{E} n_p - D_p \vec{\nabla} n_p \tag{2}$$

μ_p and D_p denote here the mobility and diffusion coefficient of species p. For the electrons also the electron energy balance equation is solved. The assumption that the energy is directly related to the local electric field is not valid for electrons because they have much lower mass compared with the heavy particles. Electron parameters are therefore expressed as a function of the average energy $\bar{\varepsilon}$ which results from this balance equation:

$$\frac{\partial (n_e \bar{\varepsilon})}{\partial t} + \vec{\nabla} \cdot \vec{\Gamma}_{\bar{\varepsilon}} = S_{\bar{\varepsilon}} \tag{3}$$

$S_{\bar{\varepsilon}}$ is again a source term which depends on the heating by the electric field and on the energy gained or lost in the various reactions. $\vec{\Gamma}_{\bar{\varepsilon}}$ denotes the electron energy flux which can be obtained from:

$$\vec{\Gamma}_{\bar{\varepsilon}} = -\frac{5}{3} \mu_e \vec{E} n_e \bar{\varepsilon} - \frac{5}{3} n_e D_e \vec{\nabla} \bar{\varepsilon} \tag{4}$$

The first term is the hydrodynamic flux of enthalpy and the second term is the heat conduction flux.

This set of partial differential equations is coupled to the Poisson equation, which delivers the electric field distribution:

$$\vec{\nabla} \cdot \left(\varepsilon_m \vec{\nabla} \varphi \right) = -\vec{\nabla} \cdot \left(\varepsilon_m \vec{E} \right) = -\sum_p q_p n_p \tag{5}$$

φ is here the electric potential as a function of time and space, ε_m is the permittivity of the medium (i.e., the plasma and the dielectrics), and q_p is the charge of species p. This Poisson equation is not only solved within the plasma, but also inside the dielectric, where it reduces to:

$$\nabla^2 \varphi = 0 \tag{6}$$

because no charges are present inside the dielectric.

The effect of charge accumulation on the surface of the dielectric materials is considered using Gauss's law:

$$\varepsilon_{\text{dielectric}} \vec{E}_{\text{dielectric}} \cdot \vec{u_n} - \varepsilon_{\text{gas}} \vec{E}_{\text{gas}} \cdot \vec{u_n} = \sigma \tag{7}$$

where $\vec{E}_{\text{dielectric}}$ and $\vec{E}_{\text{gas}}$ are the electric field inside the dielectric and in the gas, respectively, $\vec{u_n}$ is the unit vector normal to the wall, where the charge accumulation occurs.

σ is the surface charge density on the dielectric, calculated from the charged particle fluxes directed to the surface.

Furthermore, at the open boundaries (top and bottom of the reactor) homogeneous Neumann boundary conditions are employed, meaning that the derivatives of the plasma quantities in the direction perpendicular to these boundaries are set to zero; this applies to the densities of all the active species, the electron energy density and the potential distribution. At the physical boundaries, i.e., the electrodes and the dielectric, the boundary conditions for n_i and n_e are given by the expressions for the flux densities $\vec{\Gamma}_i$ and $\vec{\Gamma}_e$. These boundary conditions are determined by the reflection coefficients and the secondary electron emission coefficients of the different species included in the model. Besides, the correct electrode properties and dielectric properties are defined in the model. Detailed information about the boundary conditions can be found in ref.[75]

The coupled differential equations are solved by the so-called "modified strongly implicit method,"[76] using an extra stabilization method,[58] until convergence is reached over the discharge cycles.

The electron transport parameters and rate coefficients are not updated with each iteration, but they are updated whenever the densities of the molecules change a few percent.

A more detailed description of the physics used in the model and of the numerical methods that are used is reported by Hagelaar[58] and by Brok et al.[62]

Because the aim of our research is to determine the conversion of CH_4 and the yields of the reaction products, calculations are carried out for a residence time up to 20 s. To limit the calculation time, the fluid model is used to follow all species as a function of time with a maximal time step in the order of 10 ns, until a periodic steady state is reached for the charged species. This takes typically 2 ms or 20 periods. Subsequently, the time averaged electron density, electron energy, and rate coefficients of electron impact reactions are calculated and taken as a constant input for a reduced fluid model in which the electron energy balance equation and the Poisson equation are not solved. In this second part the conversion of the molecules is calculated with a larger time step in the order of 100 μs. Back-coupling to the short time step calculations is carried out regularly, to update the electron energy and density and the rate coefficients of the electron impact reactions if necessary. In this way the calculation speed could be increased with a factor of 10^4.

Figure 1. Schematic diagram of the reactor under study.

Reactor Set-Up

The numerical model is applied to an atmospheric pressure CH_4 cylindrical DBD (see Figure 1). The reactor consists of two coaxial electrodes. The inner electrode (stainless steel) has an outer diameter of 22 mm. The outer electrode (chrome) has a diameter of 29.3 mm and at the inside it is in contact with a dielectric tube made of alumina. The alumina tube has an inner diameter of 26 mm and a wall thickness of 1.6 mm leading to a discharge gap of 2 mm wide between both cylinders, i.e., the region where the gas flows through the reactor. The outer electrode is powered, whereas the inner electrode is grounded. The background gas temperature is 300 K and assumed to be constant and uniform in time and in space, respectively. This is justified because in the experiments under consideration cooling is used and so the temperature is kept constant at about 300 K. The total length of the reactor in the experiment is 120 mm. A residence time of 20 s corresponds for this set-up to a gas flow rate of about 0.05 $L \cdot min^{-1}$. More detailed information on the reactor set-up has been reported by Paulussen et al.[77]

However, in the model only a segment of 1.5 mm long is considered. This is done to limit the calculation time and to avoid having to deal with filament formation in the reactor, as this cannot yet be simulated with the present model. On the other hand, by using three grid cells, instead of one, in the axial direction it is possible to describe the boundary conditions (see above) in a proper way in both the axial and the radial direction.

It needs to be realized that the effect of gas flow in the reactor is not modeled explicitly. Indeed, the real reactor can be considered as a kind of plug flow reactor, hence the concentration of the species varies as a function of the position in the reactor when the gas flows through. However, in the model this can be approximated by considering the reactor as a batch reactor, where the

DOI: 10.1002/ppap.201100027

concentration of the species varies as a function of the residence time. Indeed, the variation of the concentrations as a function of time in a batch reactor is the same as the variation as a function of position in a plug flow reactor. In other words, the effect of gas flow is accounted for by studying the time variation of the species concentrations, where the residence time is calculated as the reactor volume divided by the gas flow rate. Experiments are performed for this DBD set-up to validate the calculated results. The analysis of the reaction product mixture is done by gas chromatography. A Trace GC from Thermo is equipped with two analysis channels. A first channel contains a thermal conductivity detector (TCD) to analyze the outcome of two serial installed packed columns: a Hayesep Q (80–100, 2 m * 1/8″ Siltek) and a Molsieve 5A (80–100, 3 m * 1/8″). The second channel has a flame ionization detector (FID) installed after a RTX-1 capillary column (5 μ, 25 m * 0.53 mm).

Species Included in the Model

In order to describe the chemistry in a pure methane plasma, 36 species (electrons, molecules, ions, and radicals) are taken into account in the model. The selection of species is based on other modeling studies for methane discharges under various conditions.[39,78,79] In addition to the feed gas CH_4, also H_2 and some higher order neutral molecules C_2H_6, C_2H_4, C_2H_2, C_2, C_3H_8, and C_3H_6 are considered in the model, as it was shown in literature that they are formed in the plasma at high densities.[29,36] High densities of C_2H_2 in the discharge may lead to polymerization and in order to deal with this in a first attempt the polymerization product C_4H_2 is also included in the model. Furthermore, 11 radical species and 16 ionic species are taken into account corresponding to the products of dissociation and ionization reactions, respectively, of these high density molecules.

A methane plasma has a very strong electropositive character. The negative ion densities are about one order of magnitude lower than the electron and the positive ion densities[40,41] and therefore, negative ions are not incorporated in the model. Although some vibrational excitation reactions are included in the model, vibrationally excited species are not taken into account separately in order to limit the number of species and reactions. Also rotationally and electronically excited species are not taken into account in the model. Indeed, the electron energy required for rotational excitations is negligible compared with this for vibrational excitations,[78,79] and all electronic excited states of methane lead to dissociation.[80] Therefore, it is also assumed here that the electronically excited states for the higher order neutrals lead to dissociation. An overview of the different species taken into account can be found in Table 1.

Transport and Wall Interaction Coefficients

The above-mentioned species are provided in the model with their transport coefficients for diffusion and mobility (only for the charged species), a sticking coefficient and a secondary electron emission coefficient.

The diffusion coefficient D_{ij} ($m^2 \cdot s^{-1}$) of the neutral species j in the background gas i is obtained by the Chapman-Enskog equation:[78,81]

$$D_{ij} = \frac{3k_b T\sqrt{\frac{4\pi k_b T}{2m_{ij}}}}{16p\pi\sigma_{ij}^2\Omega_D(\Psi)} \tag{8}$$

where k_b is the Boltzmann constant, T is the background gas temperature (K), p is the total pressure (Pa), m_{ij} is the reduced mass (kg), σ_{ij} is the characteristic length (m) and Ω_D is the dimensionless diffusion collision integral. This collision integral, which is a function of the dimensionless temperature Ψ, is given by

$$\Omega_D = \frac{A}{\Psi^B} + \frac{C}{e^{D\Psi}} + \frac{E}{e^{F\Psi}} + \frac{G}{e^{H\Psi}} \tag{9}$$

where Ψ equals $k_b\ T/\varepsilon_{ij}$, $A = 1.06036$, $B = 0.15610$, $C = 0.19300$, $D = 0.47635$, $E = 1.03587$, $F = 1.52996$, $G = 1.76474$, and $H = 3.89411$.[81] σ_{ij} and ε_{ij} are calculated by

$$\sigma_{ij} = \frac{\sigma_i + \sigma_j}{2} \tag{10}$$

$$\varepsilon_{ij} = \sqrt{\varepsilon_i \varepsilon_j} \tag{11}$$

Table 1. Overview of the species included in the model, besides the electrons.

Molecules	Ions	Radicals
CH_4	CH_5^+, CH_4^+, CH_3^+, CH_2^+, CH^+, C^+	CH_3, CH_2, CH, C
C_2H_6, C_2H_4, C_2H_2, C_2, C_3H_8, C_3H_6	$C_2H_6^+$, $C_2H_5^+$, $C_2H_4^+$, $C_2H_3^+$, $C_2H_2^+$, C_2H^+, C_2^+	C_2H_5, C_2H_3, C_2H, C_3H_7, C_3H_5
H_2	H_3^+, H_2^+, H^+	H
C_4H_2		

with $\sigma(m)$ and $\varepsilon(J)$ being the characteristic length and energy for every species in the 12-6 Lennard–Jones potential. These Lennard–Jones parameters were reported for most of the neutral species by Reid et al.[81] and by Svehla[82] and for the other species they were obtained by linear interpolation.

Finally the diffusion coefficient D_j of the species j in the entire gas mixture, i.e., the sum of all background gases i, is obtained from the different D_{ij}-values using Blanc's law:[83]

$$\frac{p_{tot}}{D_j} = \sum_i \frac{p_i}{D_{ij}} \tag{12}$$

with p_{tot} the total pressure and p_i the partial pressure of the background gas i.

The ion mobility coefficient $\mu_{i,j}$ ($m^2 \cdot V^{-1} \cdot s^{-1}$) of an ion j in the background gas i is calculated using the low electric field Langevin mobility expression:[83]

$$\mu_{i,j} = 0.515 \frac{T}{p\sqrt{m_{ij}\alpha_i}} \tag{13}$$

with T again the background gas temperature (K), p the gas pressure (Pa), m_{ij} the reduced mass (amu), and α_i the polarizability ($Å^3$) of the background gas which was obtained from Böttcher and Bordewijk.[84] Afterwards the mobility coefficient μ_j of the ion j in the entire gas mixture can be obtained in a similar way as the diffusion coefficient according to Blanc's law.

The mobility of the electrons and the rates of their collision reactions are described as parameters depending on the mean electron energy. These dependencies are calculated using the external Boltzmann solver Bolsig+,[85] which creates lookup tables for the mean electron energy, the electron mobility and the reaction rate coefficients as function of the reduced electric field. Accordingly, the electron mobility and the rate coefficients can be used as a function of the mean electron energy, which is calculated with the electron energy balance equation (see above).

From the ion mobility coefficient μ_j the ion diffusion coefficient D_j of an ion j can directly be obtained using the Einstein relation in order to remain consistent with the physical approximations used in the model:

$$D_j = \frac{k_b T_{ion}}{e} \mu_j \tag{14}$$

where k_b is again the Boltzmann constant, T_{ion} is the ion temperature (K) which is assumed to be equal to the background gas temperature and e is the elementary charge. The Einstein relation is also used to obtain the electron diffusion coefficient from the electron mobility.

The sticking coefficients for the different radicals are based on reported values by Bohmeyer et al.[86] and by Eckert et al.[87] Although the reported sticking coefficients are defined for somewhat different conditions, a good indication of the trend of the coefficients can be deduced. These sticking probabilities[86] are used in the first part of the modeling (i.e., the full fluid model), in order to calculate realistic discharge characteristics. In the second part of the modeling (i.e., the reduced fluid calculations, carried out on the longer timescale), the sticking probabilities of the radicals are assumed zero as the sticking coefficients used in the first part of the model lead to too much carbon deposition at the reactor walls when considering the gas conversion process on a longer time scale and thus to unrealistic results compared to the experiments. Furthermore, a realistic estimation or fitting of the sticking probabilities is not possible because experimental information about the gas phase density and behavior of each of the different species cannot be obtained. The sticking probabilities for the various molecules and the ions were assumed to be zero and one, respectively. Note that the description of the surface reactions in the model is currently limited to this rough approximation and therefore the calculated densities of the radicals and molecules might be overestimated. The calculated densities of the ions, on the other hand, might be underestimated, although this is not so likely, as sticking equal to one is quite realistic for the ions, because they are indeed mostly neutralized upon arrival at the walls. For the ions, also secondary electron emission is considered when they collide with the reactor wall.

Chemical Reactions

A consistent set of 367 gas phase reactions involving the 36 defined species was built to describe the plasma chemistry in the discharge gap. These gas phase reactions can be divided into four groups: 100 electron–neutral, 35 electron–ion, 92 neutral–neutral, and 140 ion–neutral reactions. The electron–neutral reactions include 6 momentum transfer, 15 vibrational excitation, 47 ionization, and 32 dissociation reactions. The electron–ion reactions are all dissociative recombination reactions, because volume recombination is an important process at atmospheric pressure. An overview of the reactions considered in the model is given in the Appendix.

The rates of the different reactions are calculated in the model from the densities of the colliding species and the corresponding reaction rate coefficients. For the electron–neutral and electron–ion reactions an energy dependent reaction rate coefficient is used. The previously mentioned Boltzmann solver Bolsig+ is used to create the lookup tables for the rate coefficients of the electron–neutral reactions based on the energy dependent collision cross sections for these reactions. The references for the cross sections can also be found in Table A.1 of the Appendix. The lookup

DOI: 10.1002/ppap.201100027

tables for the electron–ion dissociative recombination reactions are built using the functions in combination with the branching ratios for the different channels of which a detailed overview is given in Table A.2 of the Appendix. The neutral–neutral and ion–neutral reactions are defined in the model with a constant reaction rate coefficient for the working pressure and temperature of 1 atm and 300 K, respectively. The constant rate coefficients and their corresponding references for the neutral–neutral and ion–neutral reactions are summarized in Table A.3 and Table A.4, respectively. Note that the rate coefficient of the recombination reaction of CH_3 with C_2H_5 resulting in the formation of C_3H_8 was estimated based on the matching between experimental results and our calculation results. The values reported in literature for this reaction are either too low[88] (i.e., $5.60 \times 10^{-11}\,cm^3 \cdot s^{-1}$, which is equal to $2.29 \times 10^{-30}\,cm^6 \cdot s^{-1}$ as adjusted for a three-body collision by dividing by the density of the background gas) or too high[89] (i.e., $1.87 \times 10^{-23}\,cm^6 \cdot s^{-1}$). Therefore a rate coefficient of $1 \times 10^{-28}\,cm^6 \cdot s^{-1}$ is assumed in the model.

Results and Discussion

The calculations are carried out at a fixed applied voltage of 6 kV and a frequency of 10 kHz, which are typical operating conditions applied in the experiments.[77] First, the densities of the various plasma species will be shown. Subsequently, the conversion of the background gas and the yields and selectivities of the formed end products will be discussed. Finally, the dominant reaction pathways governing the conversion process will be pointed out.

Densities of the Plasma Species

Figure 2 illustrates the periodic behavior of the spatially averaged electron density on a linear (a) and on a logarithmic (b) scale as a function of time, for four periods of the applied voltage. The applied voltage as a function of time is also plotted. It is clear that multiple breakdowns in the gas appear each half period following the applied voltage. The difference in the electron density behavior for the positive and the negative polarity of the applied voltage is due to the dissimilarity in surface dimensions and properties of the inner and outer electrode (only one of the electrodes is covered by a dielectric, see Figure 1 above). The overall spatially and time averaged electron density amounts to $10^{17}\,m^{-3}$. The overall spatially and time averaged electron energy was calculated to be about 2 eV.

Note that the present model cannot deal with filament formation in the reactor. Therefore, the shown electric behavior corresponds to a DBD treated as a homogeneous glow discharge. Of course, this behavior is quite different from the experimental behavior, but we believe that the rest of our calculation results, such as conversion and yields, and the reaction pathways, are still valid.

The spatial variation of the electron density, total ion density and electron energy, taken at the maximum of its time profile, is depicted in Figure 3. It is clear that in the bulk plasma, the electron and ion densities are in the order

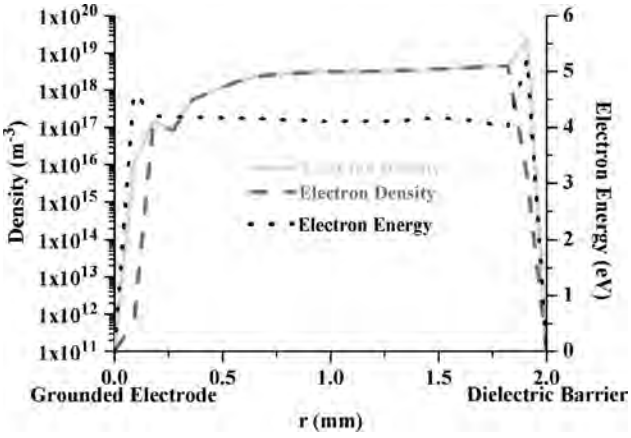

Figure 3. Calculated spatial profiles of the electron and total ion density (left axis) and electron energy (right axis) in the gap between both electrodes, taken at the maximum of their time profile. The inner (grounded) electrode is at the left, whereas the outer (powered) electrode with the dielectric layer is at the right.

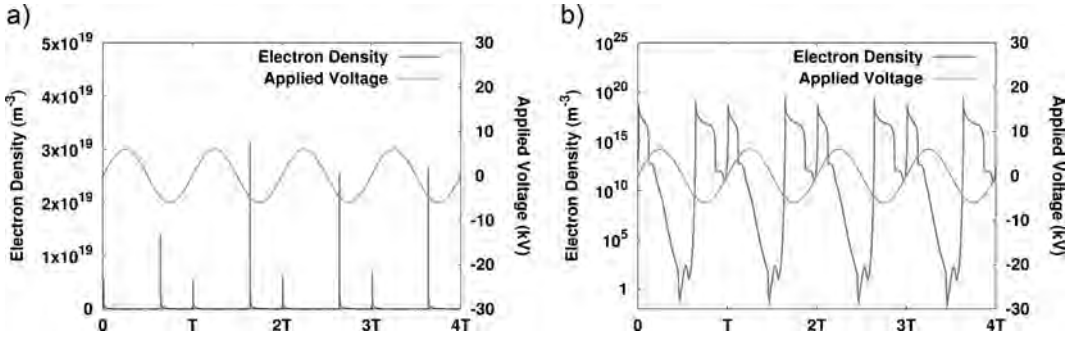

Figure 2. Spatially averaged electron density, on a linear (a) and a logarithmic (b) scale, as a function of time, as well as the applied voltage for four periods of time.

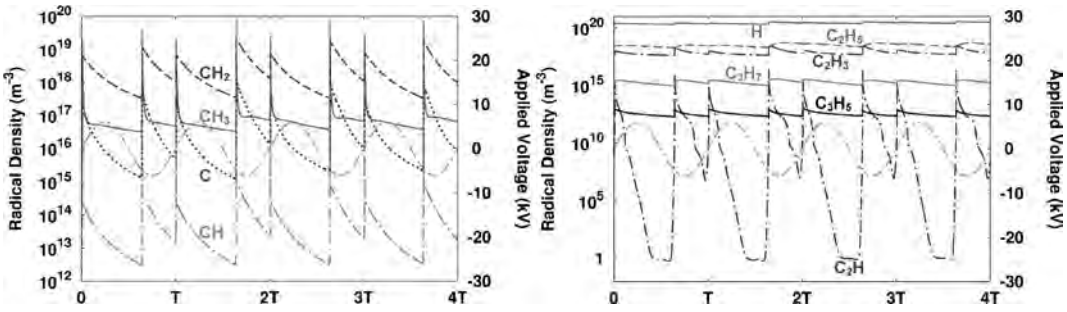

Figure 4. Spatially averaged radical densities (left axis) as a function of time, as well as the applied voltage (sinusoid, gray, right axis) for four periods of time.

of $10^{18}\,m^{-3}$, and they are more or less equal to each other, providing charge neutrality in the bulk. However, close to the electrodes, the electron density drops to zero, and the total positive ion density is several orders of magnitude higher than the electron density, providing a net positive space charge. This behavior is typical for the sheath formation in a DBD.[90] A different behavior is observed in the pre-sheath near the inner (grounded) electrode, where the ion density drops one order of magnitude, while near the dielectric barrier at the outer (powered) electrode the ion density rises one order of magnitude. This different behavior is attributed to the fact that at this particular moment in time the powered electrode (covered by the dielectric barrier) is the cathode, which attracts the ions, while the grounded electrode is the anode, which repels the ions. Due to the acceleration of the electrons in the high electric field in the sheath these electrons have an increased energy there.

Collisions of the electrons with the background gas molecules lead to the formation of radicals and ions. The number densities of these radicals and ions exhibit the same periodic behavior as the electron density. Figure 4 shows the spatially averaged radical densities as a function of time. In case of the radicals this periodic trend is superimposed on a rising or declining trend which acts over a longer time scale until periodic steady state is reached. The variation through a period, i.e., the difference between the minimum and maximum value in one period, varies from less than one order of magnitude for C_2H_5, C_2H_3, C_3H_7, C_3H_5, and H to several orders of magnitude for CH_3, CH_2, CH, C, and C_2H. This can be explained by the fact that, except for C_2H, this last group of radicals is directly formed from the background gas CH_4 by electron impact dissociation, which is not the case for the higher order radicals. The overall spatially and time averaged radical densities vary from about $10^{12}\,m^{-3}$ for the less abundant radicals to about $10^{20}\,m^{-3}$ for the most abundant radicals. The most abundant radicals are H, CH_3, CH_2, C_2H_5, and C_2H_3. The overall spatially and time averaged ion densities vary from almost zero to the order of $10^{16}\,m^{-3}$ for the most important ions (CH_5^+, $C_2H_5^+$, $C_2H_4^+$, $C_2H_3^+$).

Recombination of the radicals leads to the formation of higher order hydrocarbons and hydrogen gas. The spatially averaged densities of these molecules do not exhibit this periodic behavior. Indeed, their densities behave more or less independent from the applied voltage, since they are only indirectly correlated with the electron density and electron energy by the densities of the radicals from which they are formed (see discussion about the reaction pathways below). The net production of these higher hydrocarbon molecules and hydrogen gas is higher than their net consumption and as result a gradual increase in the densities is observed each half period of the applied voltage. In contrast, the net consumption of CH_4 is higher than its net production and therefore a gradual decrease in the CH_4 density is observed each half period. Therefore, it is more interesting to look to the variation of the molecule densities on a longer time scale.

Figure 5 illustrates the spatially averaged molecule densities as a function of the residence time in the plasma reactor. Note that a residence time of 20 s corresponds to a gas flow rate of $0.05\,L\cdot min^{-1}$ for the experimental set-up

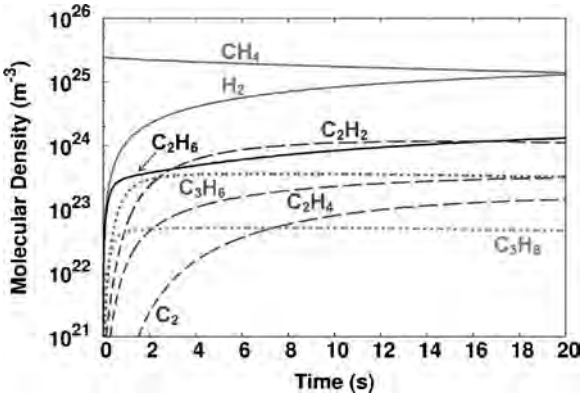

Figure 5. Spatially averaged molecular densities as a function of the residence time.

DOI: 10.1002/ppap.201100027

under study (see above). The density of the background gas methane is initially $2.45 \times 10^{25}\,m^{-3}$, but is decreasing due to dissociation and ionization reactions governing the conversion process. As a result H_2, C_2H_6, C_2H_4, C_2H_2, C_2, C_3H_8, and C_3H_6 are formed and are also present in the discharge at high densities, as shown in Figure 5. It appears that the production is most pronounced in the first 1–2 s and that the densities of the higher hydrocarbons and H_2 molecules do not significantly change anymore for a longer residence time. However, the logarithmic scale is a bit misleading and the conversion still continues, as will be illustrated below. The spatially averaged densities vary between 10^{22} and $10^{25}\,m^{-3}$ for the different molecules. H_2 seems to be formed at the highest density, and after 20 s, its density is comparable to the CH_4 density. As far as the higher hydrocarbon species are concerned, it appears from Figure 5 that C_2H_6 and C_2H_2 are formed with the highest density, which is only about one order of magnitude lower than the CH_4 density after 20 s. As a result of the polymerization of C_2H_2, also C_4H_2 is formed with a density of $10^{24}\,m^{-3}$. At first sight, this density seems rather high. This can be explained by the fact that C_4H_2 is considered in the model as the sum of all higher polymerized species. Moreover, in the model no loss mechanism for C_4H_2 is included and the sticking probability of C_4H_2 is defined zero as for the other molecules (see above).

Conversion of CH_4, and Yields and Selectivities of the Reaction Products

This model can also calculate the conversion, yields and selectivities of the molecules, which is of interest from application point of view. The definitions of the conversion X, the yields Y and the selectivities S, as used in this paper, are as follows. In these definitions the parameter x denotes the stoichiometric balance coefficient, which corresponds also to the index in the compound name of C_xH_y:

$$X_{CH_4} = \frac{n_{CH_4,\text{converted}}}{n_{CH_4,\text{feed}}} \times 100\,\% \tag{15}$$

$$Y_{H_2} = \frac{n_{H_2}}{2 \times n_{CH_4,\text{feed}}} \times 100\,\% \tag{16}$$

$$Y_{C_xH_y} = \frac{x \times n_{C_xH_y}}{n_{CH_4,\text{feed}}} \times 100\,\% \tag{17}$$

$$S_{H_2} = \frac{n_{H_2}}{2 \times n_{CH_4,\text{converted}}} \times 100\,\% \tag{18}$$

$$S_{C_xH_y} = \frac{x \times n_{C_xH_y}}{n_{CH_4,\text{converted}}} \times 100\,\% \tag{19}$$

Figure 6a illustrates the calculated conversion of CH_4 and the yields of the reaction products, i.e., H_2 and the summation over all C_2H_y and C_3H_y hydrocarbons, as a function of residence time in the reactor (solid lines). The measured conversion and yields of these products, for similar operating conditions, are depicted with dashed lines.

As expected, both the conversion and the various yields increase as a function of residence time. After 20 s, only 40% of CH_4 is converted and the H_2 and C_2H_y molecules are formed with the highest yields. Reasonable agreement is reached between calculated and experimental results, taking into account the complexity of the plasma chemistry. The calculated and measured CH_4 conversion and C_3H_y yield agree within 5%. However, the differences are significant for the H_2 yield and the C_2H_y yield, although they show at least similar trends between calculated and experimental values. A possible explanation for these significant differences is given below when the selectivities of H_2 and C_2H_2 are discussed. The calculated and measured carbon and hydrogen balances are plotted in Figure 6b and show an agreement within 20%. A possible explanation for the differences between the calculated and the measured balances is the uncertainty of the used sticking coefficients. The carbon balance drops slightly as a function of residence time, due to sticking at the walls in the form of solid carbon. After a residence time of 20 s, roughly 20% of the carbon atoms is left in the reactor.

In Figure 6c, the calculated (solid lines) and measured (dashed lines) selectivities of the individual reaction products are plotted as a function of the conversion of CH_4. From the higher hydrocarbons, C_2H_6 (dark blue) has the highest selectivity, both in the calculated and the measured results. The selectivity is especially high (100% in the calculations) at very low conversion of CH_4. This is because when the discharge is ignited, electron impact dissociation of CH_4 leads to the formation of H_2 and CH_3. This methyl radical will immediately initiate the recombination reactions towards C_2H_6, which in turn is converted later in new radicals and the other higher hydrocarbons. A more thorough discussion on the dominant reaction pathways can be found in the next section. However, this very low conversion is not interesting from an applications point of view. The typical selectivity, in the range of 10–40% CH_4 conversion, is around 20–30%.

The experimental results show that C_2H_4 (dark cyan, dashed) and C_2H_2 (red, dashed) have a much lower selectivity than C_2H_6. The calculated selectivity of C_2H_4 (dark cyan, solid) is in good agreement with the experiment (i.e., in the order of 5–10%), but the calculated selectivity of C_2H_2 (red, solid) is too high compared to the experimental results. A possible reason might be that the further polymerization of C_2H_2 molecules into higher molecules is underestimated in the model. Indeed, dust formation appears to be important in acetylene plasmas. In previous models by our group,[91–93] these polymerization reactions

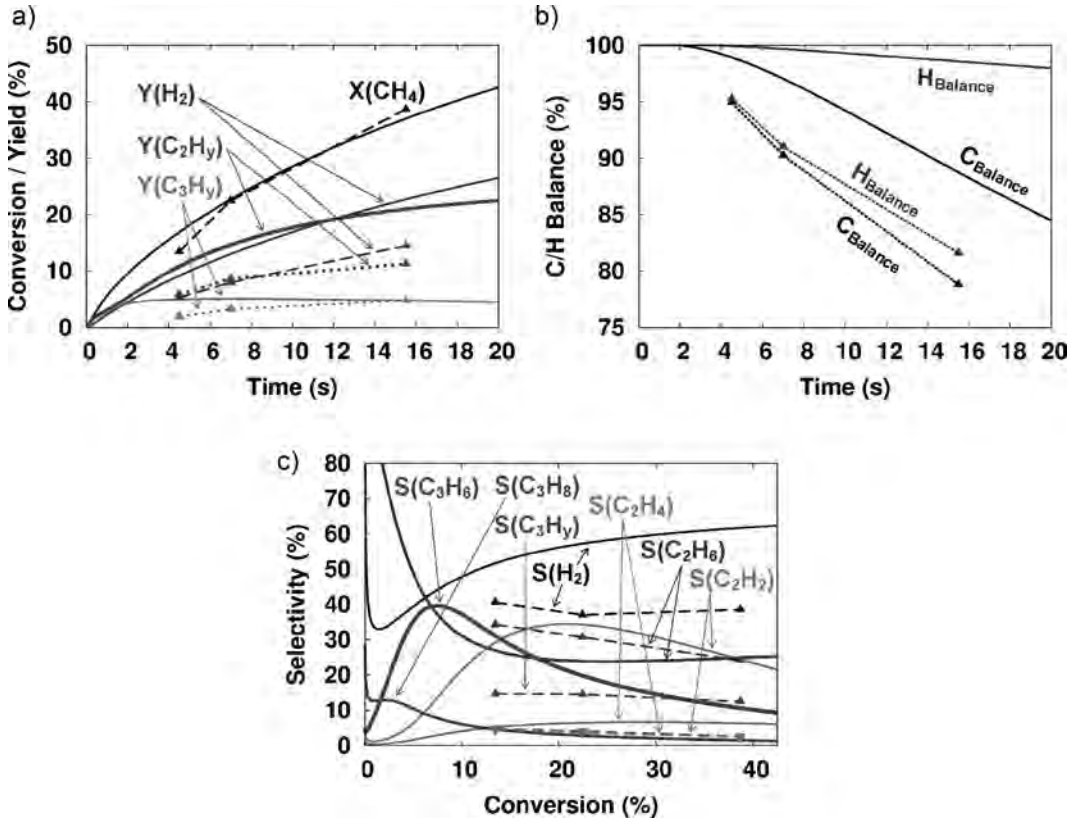

Figure 6. (a) Calculated (solid lines) and experimental (dashed lines) conversion of CH_4 and yields of the reaction products, as a function of residence time in the reactor. (b) The calculated (solid lines) and measured (dashed lines) carbon-balances and hydrogen-balances are illustrated. (c) The calculated (solid lines) and experimental (dashed lines) selectivities of the individual hydrocarbon reaction products are plotted as a function of the conversion of CH_4. Note that the selectivity of C_3H_6 could not be measured.

were studied in detail by an extensive chemistry set, including neutral, positive, and negative ion pathways. However, in the present model, the polymerization is only treated by one chemical reaction (i.e., C_2H insertion; see below), in order not to further complicate our plasma chemistry set, which is already huge. Therefore, the obvious overestimated C_2H_2 selectivity in our model is probably attributed to the underestimation of C_2H_2 polymerization. Moreover, the overestimated C_2H_2 formation explains why the calculated yield of the overall C_2H_y fraction is higher than the measured values (Figure 6a).

The calculated and measured yields of the summation over all C_3H_y molecules are in an almost perfect agreement (Figure 6a). The sum of the calculated selectivities of C_3H_8 (dark green, solid) and C_3H_6 (light green, solid) is in reasonable agreement with the total measured selectivity of C_3H_y (green, dashed). However, it is not possible to compare the calculated selectivities of the different compounds as the measured peaks of the different C_3H_y molecules overlap in the chromatogram.

Besides the higher hydrocarbons, H_2 is also formed as a main end product in the discharge. The calculated yields and selectivities of H_2 are a bit higher than the measured values. This is probably because the production of H_2 by electron impact dissociation of C_2H_6 and C_3H_8 (see next section for the most important consumption and production pathways of H_2) is assumed a bit too high in the model.

As mentioned above, the formation of C_4H_2 by polymerization reactions of C_2H_2 species is also included in the model. However, as C_4H_2 could not be measured in the experiments, it is treated as a loss of carbon in the model in order to match the calculated and measured carbon balances. The calculated yield of C_4H_2 after 20 s amounts to 13.75%.

Reported results in the literature based on experiments on the conversion of methane into higher hydrocarbons, at similar conditions, show similar trends, namely the end products were mainly H_2 and C_2H_y (mostly C_2H_6) as well as, to a lower extent, some higher hydrocarbons (C_3H_y, C_4H_y, ...).[5,29,36]

DOI: 10.1002/ppap.201100027

Dominant Reaction Pathways

Electron Impact Reactions With CH_4: The Formation of Radicals and Ions

As soon as the sinusoidal voltage is applied to the reactor and the discharge is ignited, electron impact ionization and dissociation of CH_4 occurs and this results in the consumption of CH_4 and the creation of new species (electrons, ions, radicals). The formation of new electrons and ions in the plasma is important in order to sustain the discharge. The most important channels for electron impact ionization of CH_4 are:

$$e^- + CH_4 \rightarrow 2e^- + CH_4{}^+ \quad \text{(R1)}$$

$$e^- + CH_4 \rightarrow 2e^- + CH_3{}^+ + H \quad \text{(R2)}$$

Our calculations point out that reaction (R1) is responsible for 66% of the total electron impact ionization of CH_4, while reaction (R2) is responsible for 33%, which is in good agreement with the results reported by Yang.[48]

The dissociation of CH_4 leads to the formation of radicals. It is of special interest when studying the gas conversion process, because these radicals are important reagents in the production of higher order hydrocarbons. The most important channels for consumption of CH_4 are electron impact dissociation reactions, more specifically:

$$e^- + CH_4 \rightarrow e^- + CH_3 + H \quad \text{(R3)}$$

$$e^- + CH_4 \rightarrow e^- + CH_2 + H_2 \quad \text{(R4)}$$

$$e^- + CH_4 \rightarrow e^- + CH + H_2 + H \quad \text{(R5)}$$

Our calculations point out that reaction (R3) is responsible for 79% of the total electron impact dissociation of CH_4, while reaction (R4) and (R5) are responsible for 15 and 5%, respectively. Similar results were reported by Yang.[48]

The dominant reactions for CH_4 consumption (and production) are depicted in Figure 7a. It is clear that the electron impact dissociation reaction to CH_3 (i.e., reaction (R3)) is by far the dominant consumption process of CH_4, followed by electron impact ionization to CH_4^+ (i.e., reaction (R1)). Besides the electron impact ionization and dissociation reactions, also some neutral–neutral and ion–neutral reactions are important for the consumption of CH_4 (see Figure 7a).

Note that electron impact vibrational excitation of CH_4 is also an important process. However, in the model these vibrational excitation reactions are only considered as an energy loss for the electrons (i.e., the vibrationally excited species are not taken into account separately) and therefore these reactions are not included in Figure 7a since they neither entail consumption or production of CH_4. In literature it is reported that a similar result is obtained whether the vibrationally excited species are taken into account or not, because in that case the electron impact excitation to $CH_4{}^*$ is balanced by the de-excitation of $CH_4{}^*$ on the reactor wall.[48]

It can also be deduced from Figure 7a that the most important pathways for the regeneration of CH_4 are based on electron impact dissociation of higher hydrocarbons, such as C_3H_6 and C_3H_8 (see below).

The Recombination of CH_3: The Formation and Loss of C_2H_6 and C_3H_8

The most important radical produced out of CH_4 is CH_3, which is mainly formed by reaction (R3) above. This radical will initiate the recombination reactions towards higher hydrocarbons such as C_2H_6 and especially C_3H_8:

$$CH_3 + CH_3 + CH_4 \rightarrow C_2H_6 + CH_4 \quad \text{(R6)}$$

$$CH_3 + C_2H_5 + CH_4 \rightarrow C_3H_8 + CH_4 \quad \text{(R7)}$$

The most important pathways for the production and consumption of ethane (C_2H_6), which is mainly used in the chemical industry as a feedstock for the production of ethylene (C_2H_4), and propane (C_3H_8), which is mainly used as a fuel source (for instance in LPG (liquefied petroleum gas), used as vehicle fuel) are illustrated in Figure 7b and c, respectively. It is clear that reaction (R7) is the dominant production process for C_3H_8 (see Figure 7c), but reaction (R6) is only responsible for about 11% of the C_2H_6 production. Indeed, as is apparent from Figure 7b, C_2H_6 is mainly (83%) formed by the recombination of two C_2H_5 radicals:

$$C_2H_5 + C_2H_5 \rightarrow C_2H_6 + C_2H_4 \quad \text{(R8)}$$

This results from the fact that the overall averaged density of C_2H_5 ($7 \times 10^{20}\,m^{-3}$) is three orders of magnitude higher than the CH_3 density, while the rate coefficient of reaction (R6) (i.e., $1.56 \times 10^{-38}\,m^6 \cdot s^{-1}$ or $3.82 \times 10^{-13}\,m^3 \cdot s^{-1}$ for a CH_4 gas density of $2.446 \times 10^{25}\,m^{-3}$) is five orders of magnitude higher than the rate coefficient of reaction (R8) (i.e., $2.41 \times 10^{-18}\,m^3 \cdot s^{-1}$). Taking into account that the rates of both reactions depend on the square of the concentrations of CH_3 and C_2H_5, respectively, it is clear that the rate of reaction (R8) is almost one order of magnitude higher than the rate of reaction (R6).

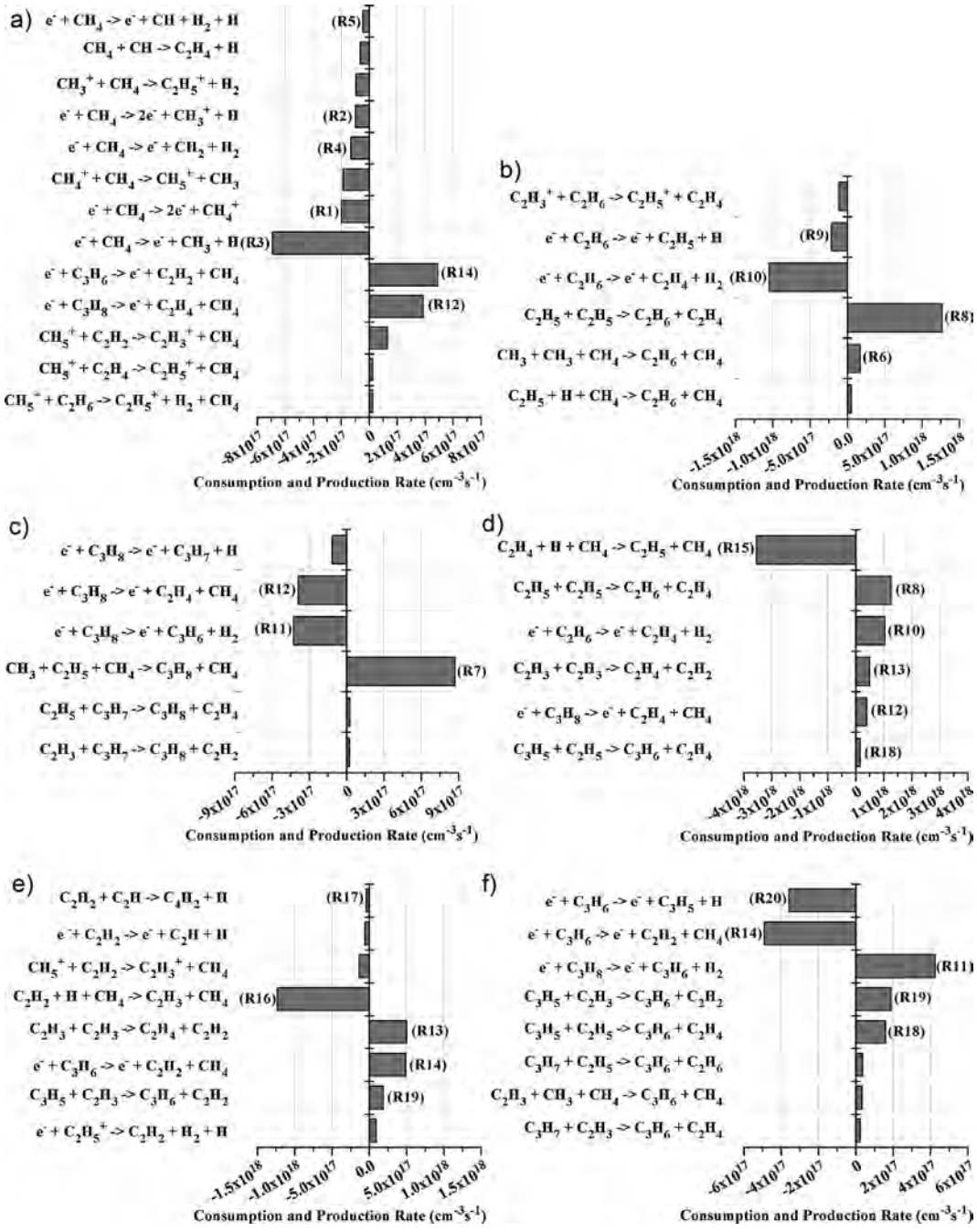

Figure 7. Calculated time-averaged reaction rates of the dominant reaction pathways for the production and consumption of CH_4 (a), C_2H_6 (b), C_3H_8 (c), C_2H_4 (d), C_2H_2 (e), and C_3H_6 (f). The production rates are plotted as positive values (i.e., right-hand side of the figures), whereas the consumption rates are defined as negative values (i.e., left-hand side of the figures). The most important pathways are labeled, and the labels correspond to the reactions given in the text.

Electron impact dissociation reactions are the most important loss processes for both C_2H_6 and C_3H_8, leading to the formation of C_2H_4, C_2H_5, and C_3H_6:

$$e^- + C_2H_6 \rightarrow e^- + C_2H_5 + H \quad \text{(R9)}$$

$$e^- + C_2H_6 \rightarrow e^- + C_2H_4 + H_2 \quad \text{(R10)}$$

$$e^- + C_3H_8 \rightarrow e^- + C_3H_6 + H_2 \quad \text{(R11)}$$

$$e^- + C_3H_8 \rightarrow e^- + C_2H_4 + CH_4 \quad \text{(R12)}$$

Especially reaction (R10) is important as loss process for C_2H_6 (see Figure 7b), whereas both reaction (R11) and

DOI: 10.1002/ppap.201100027

(R12) contribute nearly equally in the loss of C_3H_8 (see Figure 7c).

The Formation and Loss of Higher Order Unsaturated Hydrocarbons: C_2H_4, C_2H_2, and C_3H_6

The most important pathways for the production and consumption of C_2H_4, C_2H_2, and C_3H_6 are plotted in Figure 7d, e, and f, respectively. Ethylene (C_2H_4) is the most important feedstock in the chemical industry; it is mainly used for the formation of polyethylenes, which are the world's most widely used plastics. Besides, it also forms the basis for the formation of ethylene oxide, which is used in surfactants, and for the formation of ethylene glycol, which is applied as automotive antifreeze, and for many other applications. Acetylene (C_2H_2) is mainly utilized as a fuel source and as a chemical building block for the formation of ethylene and different polymerization products which are applied in the plastic industry. Propylene (C_3H_6) forms the basis for the formation of polypropylene, which is typically used in the manufacturing of packaging and textiles.

The production of C_2H_4 occurs mainly by the recombination of two C_2H_5 radicals (i.e., reaction (R8) above) and by electron impact dissociation of C_2H_6 (i.e., reaction (R10) above). Also electron impact dissociation of C_3H_8 (i.e., reaction (R12) above) and the recombination of two C_2H_3 radicals (reaction (R13)) contribute to some extent:

$$C_2H_3 + C_2H_3 \rightarrow C_2H_4 + C_2H_2 \quad \text{(R13)}$$

The latter reaction, as well as the electron impact dissociation of C_3H_6, are mainly responsible for the production of C_2H_2:

$$e^- + C_3H_6 \rightarrow e^- + C_2H_2 + CH_4 \quad \text{(R14)}$$

Hydrogen attachment reactions are the most important loss processes for both C_2H_4 and C_2H_2, leading to the formation of C_2H_5 and C_2H_3 radicals, respectively:

$$C_2H_4 + H + CH_4 \rightarrow C_2H_5 + CH_4 \quad \text{(R15)}$$

$$C_2H_2 + H + CH_4 \rightarrow C_2H_3 + CH_4 \quad \text{(R16)}$$

Note in Figure 7e also the occurrence of the polymerization reaction of C_2H_2 resulting in the formation of C_4H_2:

$$C_2H_2 + C_2H \rightarrow C_4H_2 + H \quad \text{(R17)}$$

Finally, the production of C_3H_6 occurs mainly by electron impact dissociation of C_3H_8 (i.e., reaction (R11) above) and to a lower extent also by the recombination of C_3H_5 radicals with either C_2H_5 or C_2H_3:

$$C_3H_5 + C_2H_5 \rightarrow C_3H_6 + C_2H_4 \quad \text{(R18)}$$

$$C_3H_5 + C_2H_3 \rightarrow C_3H_6 + C_2H_2 \quad \text{(R19)}$$

The loss of C_3H_6 is mainly attributed to electron impact dissociation reactions, leading to the formation of either C_2H_2 (reaction (R14) above) or C_3H_5:

$$e^- + C_3H_6 \rightarrow e^- + C_3H_5 + H \quad \text{(R20)}$$

The Role of C_2H_5: An Important Radical in the Conversion Process

Our calculations predict that C_2H_5 is present in the discharge at rather high density (see Figure 4 above), and it plays a significant role in the production and loss of the various hydrocarbon molecules. Therefore, the most important pathways for the production and consumption of this radical are illustrated in Figure 8. C_2H_5 is mainly (94%) formed by hydrogen attachment to C_2H_4 (reaction (R15)) and to a lower extent (6%) also by electron impact dissociation of C_2H_6 (reaction (R9)). The loss of C_2H_5 is mainly attributed to radical recombination by reaction (R8), (R7), and (R18) which contribute for 51, 35, and 6%, respectively. As these reactions result in the formation of C_2H_4, C_2H_6, C_3H_6, and C_3H_8, this means that the equilibrium established between C_2H_4, C_2H_5, and C_2H_6, which relies on the accuracy of the rate coefficients considered, plays a crucial role.

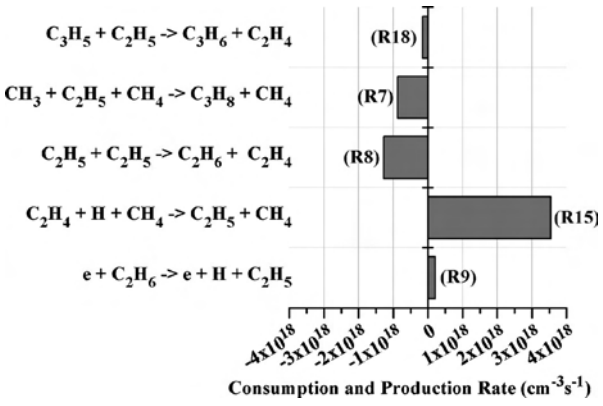

Figure 8. The dominant reaction pathways for the production and consumption of C_2H_5. The time-averaged production rates are plotted as positive values (i.e., right-hand side of the figure), whereas the time-averaged consumption rates are defined as negative values (i.e., left-hand side of the figure). The most important pathways are labeled, and the labels correspond to the reactions given in the text.

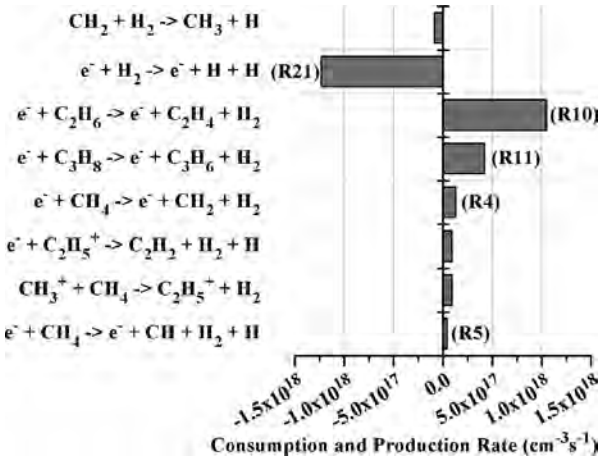

Figure 9. The dominant reaction pathways for the production and consumption of H_2. The time-averaged production rates are plotted as positive values (i.e., right-hand side of the figure), whereas the time-averaged consumption rates are defined as negative values (i.e., left-hand side of the figure). The most important pathways are labeled, and the labels correspond to the reactions given in the text.

The Formation and Loss of H_2

The most important pathways for the production and consumption of H_2 are illustrated in Figure 9. H_2 is mainly used for the processing of fossil fuels, the production of ammonia and methanol, and as fuel in fuel cells. As appears from Figure 9, H_2 is mainly produced by electron impact dissociation of hydrocarbon molecules. The dissociation reaction of C_2H_6 (reaction (R10)) appears to be the dominant production mechanism, with a contribution of 56%, whereas the dissociation of C_3H_8 (reaction (R11)) and CH_4 (reaction (R4)) contribute for 23 and 7%, respectively. Electron impact dissociation is also the dominant loss process for H_2:

$$e^- + H_2 \rightarrow e^- + H + H \qquad \text{(R21)}$$

Summary of the Dominant Pathways Governing the Conversion of CH_4 into C_xH_Y and H_2

Finally, Figure 10 gives a schematic overview of the dominant reaction pathways for the conversion of CH_4 into higher hydrocarbons and hydrogen gas. Electron impact dissociation of CH_4 resulting in the formation of the methyl radical (CH_3) starts the conversion process (R3). This methyl radical will initiate recombination reactions towards higher hydrocarbons such as C_2H_6 and C_3H_8 (R6, R7). Subsequently, a play of dissociation and recombination leads to the conversion towards the other, unsaturated hydrocarbons. Finally, dissociation of CH_4 and the higher hydrocarbons also results in the formation of H_2.

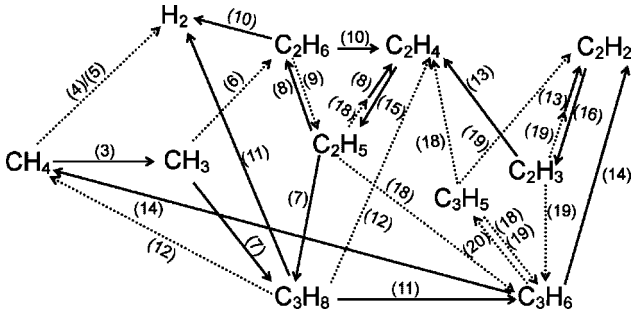

Figure 10. Schematic overview of the dominant reaction pathways for the conversion of CH_4 into higher hydrocarbons and hydrogen gas. The most important pathways are depicted with a solid line, less important channels are represented by a dashed line. The labels correspond to the reactions given in the text.

Conclusion

In this paper, a detailed plasma chemistry is presented for the conversion of CH_4 into higher hydrocarbon molecules in a DBD reactor. The densities of the various plasma species have been studied as a function of the residence time. The spatially averaged densities of the electrons, ions and radicals show a periodic behavior as a function of time, following the applied voltage. The spatially averaged densities of the molecules do not exhibit a periodic behavior. Indeed, their densities are characterized by a gradual reduction (CH_4) or increase (higher hydrocarbon molecules and H_2) each half period following the maximum of the applied voltage, which results in a more notable decreasing or increasing trend over a longer timescale.

The density of the background gas, methane, is decreasing due to dissociation (and ionization) reactions governing the conversion process. The calculated and measured conversions of CH_4 as a function of the residence time are illustrated. The dissociation of CH_4 leads to the formation of CH_3, which is the most important radical in the gas phase chemistry. This methyl radical will initiate the recombination reactions towards higher hydrocarbons. As a result, these molecules are also present in the discharge at high densities.

The calculated and measured yields and selectivities of these higher hydrocarbons (C_2H_6, C_2H_4, C_2H_2, C_3H_8, and C_3H_6) and of H_2 are depicted and a reasonable agreement between our calculation results and the measurements is established. C_2H_6 and H_2 are the main reaction products of the conversion of CH_4.

Furthermore the underlying plasma chemistry of the conversion process is analyzed and the dominant reaction pathways for the consumption of CH_4 and for the production and loss of the various end products are pointed out. It is found that electron impact dissociation of CH_4 resulting in the formation of the methyl radical (CH_3)

Plasma Process. Polym. **2011**, *8*, 1033–1058

DOI: 10.1002/ppap.201100027

initiates the conversion process. Recombination of CH_3 with either another CH_3 radical or with a C_2H_5 radical will lead to the formation of C_2H_6 and C_3H_8. Dissociation of these higher hydrocarbons leads directly to the formation of other hydrocarbons, but also indirectly by the formation of new radicals which can subsequently also recombine towards these higher order hydrocarbons. In other words, the conversion of CH_4 is a play of dissociation and recombination reactions leading to a diverse mixture of higher hydrocarbons.

Appendix: Overview of the Reactions Included in the Model

Table A.1. Electron impact reactions with the various molecules and radicals, included in the model. These reactions are treated by energy-dependent cross sections, and the references where these cross sections were adopted from, are also included. For the vibrational excitations, several individual excitations are included, as indicated by the number between brackets.

	CH_4		
Momentum transfer	$e^- + CH_4 \rightarrow e^- + CH_4$		[94]
Vibrational excitation	$e^- + CH_4 \rightarrow e^- + CH_4^*$	(2)	[94]
Ionization	$e^- + CH_4 \rightarrow 2e^- + CH_4^+$		[95]
	$e^- + CH_4 \rightarrow 2e^- + CH_3^+ + H$		[95]
	$e^- + CH_4 \rightarrow 2e^- + CH_2^+ + H_2$		[95]
Dissociation	$e^- + CH_4 \rightarrow e^- + CH_3 + H$		[96,97]
	$e^- + CH_4 \rightarrow e^- + CH_2 + H_2$		[96,97]
	$e^- + CH_4 \rightarrow e^- + CH + H_2 + H$		[96,97]
	$e^- + CH_4 \rightarrow e^- + C + 2H_2$		[96,97]
	CH_3		
Ionization	$e^- + CH_3 \rightarrow 2e^- + CH_3^+$		[95]
	$e^- + CH_3 \rightarrow 2e^- + CH_2^+ + H$		[95]
	$e^- + CH_3 \rightarrow 2e^- + CH^+ + H_2$		[95]
Dissociation	$e^- + CH_3 \rightarrow e^- + CH_2 + H$		[96,97]
	$e^- + CH_3 \rightarrow e^- + CH + H_2$		[96,97]
	CH_2		
Ionization	$e^- + CH_2 \rightarrow 2e^- + CH_2^+$		[95]
	$e^- + CH_2 \rightarrow 2e^- + CH^+ + H$		[95]
	$e^- + CH_2 \rightarrow 2e^- + C^+ + H_2$		[95]
Dissociation	$e^- + CH_2 \rightarrow e^- + CH + H$		[96,97]
	CH		
Ionization	$e^- + CH \rightarrow 2e^- + CH^+$		[95]
	$e^- + CH \rightarrow 2e^- + C^+ + H$		[95]
Dissociation	$e^- + CH \rightarrow e^- + C + H$		[96,97]
	C		
Ionization	$e^- + C \rightarrow 2e^- + C^+$		[96,97]

Table A.1. (Continued)

	C_2H_6		
Momentum transfer	$e^- + C_2H_6 \rightarrow e^- + C_2H_6$		[94]
Vibrational excitation	$e^- + C_2H_6 \rightarrow e^- + C_2H_6^*$	(3)	[94]
Ionization	$e^- + C_2H_6 \rightarrow 2e^- + C_2H_6^+$		[95]
	$e^- + C_2H_6 \rightarrow 2e^- + C_2H_5^+ + H$		[95]
	$e^- + C_2H_6 \rightarrow 2e^- + C_2H_4^+ + H_2$		[95]
	$e^- + C_2H_6 \rightarrow 2e^- + C_2H_3^+ + H_2 + H$		[95]
	$e^- + C_2H_6 \rightarrow 2e^- + C_2H_2^+ + 2H_2$		[95]
	$e^- + C_2H_6 \rightarrow 2e^- + CH_3^+ + CH_3$		[95]
Dissociation	$e^- + C_2H_6 \rightarrow e^- + C_2H_5 + H$		[98,99]
	$e^- + C_2H_6 \rightarrow e^- + C_2H_4 + H_2$		[98,99]
	C_2H_5		
Ionization	$e^- + C_2H_5 \rightarrow 2e^- + C_2H_5^+$		[95]
	$e^- + C_2H_5 \rightarrow 2e^- + C_2H_4^+ + H$		[95]
	$e^- + C_2H_5 \rightarrow 2e^- + C_2H_3^+ + H_2$		[95]
	$e^- + C_2H_5 \rightarrow 2e^- + C_2H_2^+ + H_2 + H$		[95]
Dissociation	$e^- + C_2H_5 \rightarrow e^- + C_2H_4 + H$		[98,99]
	$e^- + C_2H_5 \rightarrow e^- + C_2H_3 + H_2$		[98,99]
	C_2H_4		
Momentum transfer	$e^- + C_2H_4 \rightarrow e^- + C_2H_4$		[94]
Vibrational excitation	$e^- + C_2H_4 \rightarrow e^- + C_2H_4^*$	(2)	[94]
Ionization	$e^- + C_2H_4 \rightarrow 2e^- + C_2H_4^+$		[95]
	$e^- + C_2H_4 \rightarrow 2e^- + C_2H_3^+ + H$		[95]
	$e^- + C_2H_4 \rightarrow 2e^- + C_2H_2^+ + H_2$		[95]
Dissociation	$e^- + C_2H_4 \rightarrow e^- + C_2H_3 + H$		[98,99]
	$e^- + C_2H_4 \rightarrow e^- + C_2H_2 + H_2$		[98,99]
	C_2H_3		
Ionization	$e^- + C_2H_3 \rightarrow 2e^- + C_2H_3^+$		[95]
	$e^- + C_2H_3 \rightarrow 2e^- + C_2H_2^+ + H$		[95]
	$e^- + C_2H_3 \rightarrow 2e^- + C_2H^+ + H_2$		[95]
Dissociation	$e^- + C_2H_3 \rightarrow e^- + C_2H_2 + H$		[98,99]
	$e^- + C_2H_3 \rightarrow e^- + C_2H + H_2$		[98,99]
	C_2H_2		
Momentum transfer	$e^- + C_2H_2 \rightarrow e^- + C_2H_2$		[94]
Vibrational excitation	$e^- + C_2H_2 \rightarrow e^- + C_2H_2^*$	(3)	[94]
Ionization	$e^- + C_2H_2 \rightarrow 2e^- + C_2H_2^+$		[95]
Dissociation	$e^- + C_2H_2 \rightarrow e^- + C_2H + H$		[98,99]
	$e^- + C_2H_2 \rightarrow e^- + C_2 + H_2$		[98,99]

DOI: 10.1002/ppap.201100027

Table A.1. (*Continued*)

	C_2H		
Ionization	$e^- + C_2H \rightarrow 2e^- + C_2H^+$		[95]
Dissociation	$e^- + C_2H \rightarrow e^- + C_2 + H$		[98,99]
	$e^- + C_2H \rightarrow e^- + C + CH$		[98,99]
	C_2		
Ionization	$e^- + C_2 \rightarrow 2e^- + C_2^+$		[98,99]
Dissociation	$e^- + C_2 \rightarrow e^- + C + C$		[98,99]
	C_3H_8		
Momentum transfer	$e^- + C_3H_8 \rightarrow e^- + C_3H_8$		[94]
Vibrational excitation	$e^- + C_3H_8 \rightarrow e^- + C_3H_8^*$	(2)	[94]
Ionization	$e^- + C_3H_8 \rightarrow 2e^- + C_2H_5^+ + CH_3$		[95]
	$e^- + C_3H_8 \rightarrow 2e^- + C_2H_4^+ + CH_4$		[95]
Dissociation	$e^- + C_3H_8 \rightarrow e^- + C_3H_7 + H$		[98,99]
	$e^- + C_3H_8 \rightarrow e^- + C_3H_6 + H_2$		[98,99]
	$e^- + C_3H_8 \rightarrow e^- + C_2H_4 + CH_4$		[98,99]
	C_3H_7		
Ionization	$e^- + C_3H_7 \rightarrow 2e^- + C_2H_5^+ + CH_2$		[98,99]
	$e^- + C_3H_7 \rightarrow 2e^- + C_2H_4^+ + CH_3$		[98,99]
	$e^- + C_3H_7 \rightarrow 2e^- + C_2H_3^+ + CH_4$		[98,99]
	$e^- + C_3H_7 \rightarrow 2e^- + CH_3^+ + C_2H_4$		[98,99]
Dissociation	$e^- + C_3H_7 \rightarrow e^- + C_3H_6 + H$		[98,99]
	$e^- + C_3H_7 \rightarrow e^- + C_3H_5 + H_2$		[98,99]
	$e^- + C_3H_7 \rightarrow e^- + C_2H_4 + CH_3$		[98,99]
	$e^- + C_3H_7 \rightarrow e^- + C_2H_3 + CH_4$		[98,99]
	C_3H_6		
Ionization	$e^- + C_3H_6 \rightarrow 2e^- + C_2H_5^+ + CH$		[98,99]
	$e^- + C_3H_6 \rightarrow 2e^- + C_2H_4^+ + CH_2$		[98,99]
	$e^- + C_3H_6 \rightarrow 2e^- + C_2H_3^+ + CH_3$		[98,99]
	$e^- + C_3H_6 \rightarrow 2e^- + C_2H_2^+ + CH_4$		[98,99]
	$e^- + C_3H_6 \rightarrow 2e^- + CH_3^+ + C_2H_3$		[98,99]
Dissociation	$e^- + C_3H_6 \rightarrow e^- + C_3H_5 + H$		[98,99]
	$e^- + C_3H_6 \rightarrow e^- + C_2H_2 + CH_4$		[98,99]
	C_3H_5		
Ionization	$e^- + C_3H_5 \rightarrow 2e^- + C_2H_3^+ + CH_2$		[98,99]
	$e^- + C_3H_5 \rightarrow 2e^- + C_2H_2^+ + CH_3$		[98,99]
	$e^- + C_3H_5 \rightarrow 2e^- + CH_3^+ + C_2H_2$		[98,99]
Dissociation	$e^- + C_3H_5 \rightarrow e^- + C_2H_2 + CH_3$		[98,99]

Table A.1. (*Continued*)

	H_2		
Momentum transfer	$e^- + H_2 \rightarrow e^- + H_2$		[100]
Vibrational excitation	$e^- + H_2 \rightarrow e^- + H_2^*$	(3)	[101]
Ionization	$e^- + H_2 \rightarrow 2e^- + H_2^+$		[102]
Dissociation	$e^- + H_2 \rightarrow e^- + 2H$		[103]
	H		
Ionization	$e^- + H \rightarrow 2e^- + H^+$		[102]

Table A.2. Electron–ion recombination reactions included in the model. These reactions are treated by energy-dependent rate coefficients, and the references where these rate coefficients were adopted from, are also included.

$e^- + CH_5^+ \rightarrow CH_3 + 2H$	[96,104]
$e^- + CH_5^+ \rightarrow CH_2 + H_2 + H$	[96,104]
$e^- + CH_4^+ \rightarrow CH_3 + H$	[96,104]
$e^- + CH_4^+ \rightarrow CH_2 + 2H$	[96,104]
$e^- + CH_4^+ \rightarrow CH + H_2 + H$	[96,104]
$e^- + CH_3^+ \rightarrow CH_2 + H$	[96,104]
$e^- + CH_3^+ \rightarrow CH + H_2$	[96,104]
$e^- + CH_3^+ \rightarrow CH + 2H$	[96,104]
$e^- + CH_3^+ \rightarrow C + H_2 + H$	[96,104]
$e^- + CH_2^+ \rightarrow CH + H$	[96,104]
$e^- + CH_2^+ \rightarrow C + H_2$	[96,104]
$e^- + CH_2^+ \rightarrow C + 2H$	[96,104]
$e^- + CH^+ \rightarrow C + H$	[96,104]
$e^- + C_2H_6^+ \rightarrow C_2H_5 + H$	[99]
$e^- + C_2H_6^+ \rightarrow C_2H_4 + 2H$	[99]
$e^- + C_2H_5^+ \rightarrow C_2H_4 + H$	[99]
$e^- + C_2H_5^+ \rightarrow C_2H_3 + 2H$	[99]
$e^- + C_2H_5^+ \rightarrow C_2H_2 + H_2 + H$	[99]
$e^- + C_2H_5^+ \rightarrow C_2H_2 + 3H$	[99]
$e^- + C_2H_5^+ \rightarrow CH_3 + CH_2$	[99]
$e^- + C_2H_4^+ \rightarrow C_2H_3 + H$	[99]
$e^- + C_2H_4^+ \rightarrow C_2H_2 + 2H$	[99]
$e^- + C_2H_4^+ \rightarrow C_2H + H_2 + H$	[99]
$e^- + C_2H_3^+ \rightarrow C_2H_2 + H$	[99]
$e^- + C_2H_3^+ \rightarrow C_2H + 2H$	[99]
$e^- + C_2H_2^+ \rightarrow C_2H + H$	[99]
$e^- + C_2H_2^+ \rightarrow C_2 + 2H$	[99]
$e^- + C_2H_2^+ \rightarrow 2CH$	[99]
$e^- + C_2H^+ \rightarrow C_2 + H$	[99]
$e^- + C_2H^+ \rightarrow CH + C$	[99]

DOI: 10.1002/ppap.201100027

Table A.2. (Continued)

$e^- + C_2H^+ \rightarrow 2C + H$	[99]
$e^- + C_2^+ \rightarrow 2C$	[99]
$e^- + H_3^+ \rightarrow 3H$	[104]
$e^- + H_3^+ \rightarrow H_2 + H$	[104]
$e^- + H_2^+ \rightarrow 2H$	[104]

Table A.3. Neutral–neutral reactions included in the model, as well as the corresponding rate coefficients for 300 K and the references where these data were adopted from. Note that *a*, estimated value; *b*, adjusted in the model for a three-body collision by dividing by $2.446 \times 10^{19}\,cm^{-3}$, i.e., the density of the background gas.

$CH_4 + CH_2 \rightarrow CH_3 + CH_3$	$3.01 \times 10^{-19}\,cm^3 \cdot s^{-1}$	[105]
$CH_4 + CH \rightarrow C_2H_4 + H$	$9.74 \times 10^{-11}\,cm^3 \cdot s^{-1}$	[106]
$CH_4 + C_2H_5 \rightarrow C_2H_6 + CH_3$	$1.83 \times 10^{-24}\,cm^3 \cdot s^{-1}$	[105]
$CH_4 + C_2H_3 \rightarrow C_2H_4 + CH_3$	$2.28 \times 10^{-18}\,cm^3 \cdot s^{-1}$	[105]
$CH_4 + C_2H \rightarrow C_2H_2 + CH_3$	$1.31 \times 10^{-12}\,cm^3 \cdot s^{-1}$	[105]
$CH_4 + C_3H_7 \rightarrow C_3H_8 + CH_3$	$4.38 \times 10^{-24}\,cm^3 \cdot s^{-1}$	[107]
$CH_4 + C_3H_5 \rightarrow C_3H_6 + CH_3$	$2.02 \times 10^{-31}\,cm^3 \cdot s^{-1}$	[108]
$CH_4 + H \rightarrow CH_3 + H_2$	$8.43 \times 10^{-19}\,cm^3 \cdot s^{-1}$	[106]
$CH_3 + CH_3 \rightarrow C_2H_5 + H$	$2.71 \times 10^{-19}\,cm^3 \cdot s^{-1}$	[109]
$CH_3 + CH_3 + CH_4 \rightarrow C_2H_6 + CH_4$	$1.56 \times 10^{-26}\,cm^6 \cdot s^{-1}$	[106]
$CH_3 + CH_2 \rightarrow C_2H_4 + H$	$7.01 \times 10^{-11}\,cm^3 \cdot s^{-1}$	[106]
$CH_3 + C_2H_6 \rightarrow C_2H_5 + CH_4$	$7.21 \times 10^{-21}\,cm^3 \cdot s^{-1}$	[106]
$CH_3 + C_2H_5 \rightarrow C_2H_4 + CH_4$	$1.91 \times 10^{-12}\,cm^3 \cdot s^{-1}$	[107]
$CH_3 + C_2H_5 + CH_4 \rightarrow C_3H_8 + CH_4$	$1.00 \times 10^{-28}\,cm^6 \cdot s^{-1}$	a
$CH_3 + C_2H_4 \rightarrow C_2H_3 + CH_4$	$1.94 \times 10^{-21}\,cm^3 \cdot s^{-1}$	[105]
$CH_3 + C_2H_3 \rightarrow C_2H_2 + CH_4$	$6.51 \times 10^{-13}\,cm^3 \cdot s^{-1}$	[105]
$CH_3 + C_2H_3 + CH_4 \rightarrow C_3H_6 + CH_4$	$1.20 \times 10^{-10}\,cm^3 \cdot s^{-1}$	[110]
	$4.91 \times 10^{-30}\,cm^6 \cdot s^{-1}$	b
$CH_3 + C_2H_2 \rightarrow CH_4 + C_2H$	$7.65 \times 10^{-26}\,cm^3 \cdot s^{-1}$	[105]
$CH_3 + C_3H_8 \rightarrow C_3H_7 + CH_4$	$1.02 \times 10^{-20}\,cm^3 \cdot s^{-1}$	[107]
$CH_3 + C_3H_7 \rightarrow C_3H_6 + CH_4$	$3.07 \times 10^{-12}\,cm^3 \cdot s^{-1}$	[107]
$CH_3 + C_3H_6 \rightarrow C_3H_5 + CH_4$	$1.24 \times 10^{-19}\,cm^3 \cdot s^{-1}$	[108]
$CH_3 + H_2 \rightarrow CH_4 + H$	$9.60 \times 10^{-21}\,cm^3 \cdot s^{-1}$	[106]
$CH_3 + H \rightarrow CH_2 + H_2$	$9.96 \times 10^{-22}\,cm^3 \cdot s^{-1}$	[106]
$CH_3 + H + CH_4 \rightarrow CH_4 + CH_4$	$2.97 \times 10^{-28}\,cm^6 \cdot s^{-1}$	[106]
$CH_2 + CH_2 \rightarrow C_2H_2 + 2H$	$5.27 \times 10^{-11}\,cm^3 \cdot s^{-1}$	[106]
$CH_2 + C_2H_5 \rightarrow C_2H_4 + CH_3$	$3.01 \times 10^{-11}\,cm^3 \cdot s^{-1}$	[105]
$CH_2 + C_2H_3 \rightarrow C_2H_2 + CH_3$	$3.01 \times 10^{-11}\,cm^3 \cdot s^{-1}$	[105]
$CH_2 + C_2H \rightarrow C_2H_2 + CH$	$3.01 \times 10^{-11}\,cm^3 \cdot s^{-1}$	[105]
$CH_2 + C_3H_8 \rightarrow C_3H_7 + CH_3$	$1.02 \times 10^{-20}\,cm^3 \cdot s^{-1}$	[107]
$CH_2 + C_3H_7 \rightarrow C_2H_4 + C_2H_5$	$3.01 \times 10^{-11}\,cm^3 \cdot s^{-1}$	[107]
$CH_2 + C_3H_7 \rightarrow C_3H_6 + CH_3$	$3.01 \times 10^{-12}\,cm^3 \cdot s^{-1}$	[107]
$CH_2 + C_3H_6 \rightarrow C_3H_5 + CH_3$	$3.65 \times 10^{-17}\,cm^3 \cdot s^{-1}$	[108]
$CH_2 + H_2 \rightarrow CH_3 + H$	$5.00 \times 10^{-15}\,cm^3 \cdot s^{-1}$	[105]
$CH_2 + H \rightarrow CH + H_2$	$2.01 \times 10^{-10}\,cm^3 \cdot s^{-1}$	[106]

Table A.3. (Continued)

$CH + C_2H_6 + CH_4 \rightarrow C_3H_7 + CH_4$	$2.78 \times 10^{-10}\,cm^3 \cdot s^{-1}$	[106]
	$1.14 \times 10^{-29}\,cm^6 \cdot s^{-1}$	b
$CH + H_2 \rightarrow CH_2 + H$	$6.80 \times 10^{-13}\,cm^3 \cdot s^{-1}$	[106]
$CH + H \rightarrow C + H_2$	$1.00 \times 10^{-10}\,cm^3 \cdot s^{-1}$	[111]
$C + H_2 \rightarrow CH + H$	$1.50 \times 10^{-10}\,cm^3 \cdot s^{-1}$	[112]
$C_2H_6 + C_2H_3 \rightarrow C_2H_5 + C_2H_4$	$3.39 \times 10^{-21}\,cm^3 \cdot s^{-1}$	[105]
$C_2H_6 + C_2H \rightarrow C_2H_2 + C_2H_5$	$5.99 \times 10^{-12}\,cm^3 \cdot s^{-1}$	[105]
$C_2H_6 + C_3H_7 \rightarrow C_3H_8 + C_2H_5$	$3.16 \times 10^{-22}\,cm^3 \cdot s^{-1}$	[107]
$C_2H_6 + C_3H_5 \rightarrow C_3H_6 + C_2H_5$	$2.02 \times 10^{-28}\,cm^3 \cdot s^{-1}$	[108]
$C_2H_6 + H \rightarrow C_2H_5 + H_2$	$4.96 \times 10^{-17}\,cm^3 \cdot s^{-1}$	[108]
$C_2H_5 + C_2H_5 \rightarrow C_2H_6 + C_2H_4$	$2.41 \times 10^{-12}\,cm^3 \cdot s^{-1}$	[106]
$C_2H_5 + C_2H_4 \rightarrow C_2H_6 + C_2H_3$	$4.56 \times 10^{-27}\,cm^3 \cdot s^{-1}$	[105]
$C_2H_5 + C_2H_2 \rightarrow C_2H_6 + C_2H$	$3.72 \times 10^{-30}\,cm^3 \cdot s^{-1}$	[105]
$C_2H_5 + C_2H \rightarrow C_2H_4 + C_2H_2$	$3.01 \times 10^{-12}\,cm^3 \cdot s^{-1}$	[105]
$C_2H_5 + C_3H_8 \rightarrow C_2H_6 + C_3H_7$	$3.62 \times 10^{-22}\,cm^3 \cdot s^{-1}$	[107]
$C_2H_5 + C_3H_7 \rightarrow C_3H_8 + C_2H_4$	$1.91 \times 10^{-12}\,cm^3 \cdot s^{-1}$	[107]
$C_2H_5 + C_3H_7 \rightarrow C_3H_6 + C_2H_6$	$2.41 \times 10^{-12}\,cm^3 \cdot s^{-1}$	[107]
$C_2H_5 + C_3H_6 \rightarrow C_3H_5 + C_2H_6$	$2.53 \times 10^{-20}\,cm^3 \cdot s^{-1}$	[108]
$C_2H_5 + C_3H_5 \rightarrow C_3H_6 + C_2H_4$	$5.36 \times 10^{-12}\,cm^3 \cdot s^{-1}$	[108]
$C_2H_5 + H_2 \rightarrow C_2H_6 + H$	$2.97 \times 10^{-21}\,cm^3 \cdot s^{-1}$	[105]
$C_2H_5 + H \rightarrow CH_3 + CH_3$	$5.99 \times 10^{-11}\,cm^3 \cdot s^{-1}$	[106]
$C_2H_5 + H \rightarrow C_2H_4 + H_2$	$3.01 \times 10^{-12}\,cm^3 \cdot s^{-1}$	[105]
$C_2H_5 + H + CH_4 \rightarrow C_2H_6 + CH_4$	$2.25 \times 10^{-10}\,cm^3 \cdot s^{-1}$	[113]
	$9.20 \times 10^{-30}\,cm^6 \cdot s^{-1}$	b
$C_2H_4 + C_2H \rightarrow C_2H_2 + C_2H_3$	$1.40 \times 10^{-10}\,cm^3 \cdot s^{-1}$	[110]
$C_2H_4 + H \rightarrow C_2H_3 + H_2$	$4.92 \times 10^{-21}\,cm^3 \cdot s^{-1}$	[105]
$C_2H_4 + H + CH_4 \rightarrow C_2H_5 + CH_4$	$3.66 \times 10^{-30}\,cm^6 \cdot s^{-1}$	[106]
$C_2H_3 + C_2H_3 \rightarrow C_2H_4 + C_2H_2$	$1.60 \times 10^{-12}\,cm^3 \cdot s^{-1}$	[105]
$C_2H_3 + C_2H \rightarrow C_2H_2 + C_2H_2$	$1.60 \times 10^{-12}\,cm^3 \cdot s^{-1}$	[105]
$C_2H_3 + C_3H_8 \rightarrow C_2H_4 + C_3H_7$	$3.40 \times 10^{-21}\,cm^3 \cdot s^{-1}$	[107]
$C_2H_3 + C_3H_7 \rightarrow C_3H_8 + C_2H_2$	$2.01 \times 10^{-12}\,cm^3 \cdot s^{-1}$	[107]
$C_2H_3 + C_3H_7 \rightarrow C_3H_6 + C_2H_4$	$2.01 \times 10^{-12}\,cm^3 \cdot s^{-1}$	[107]
$C_2H_3 + C_3H_6 \rightarrow C_3H_5 + C_2H_4$	$6.58 \times 10^{-19}\,cm^3 \cdot s^{-1}$	[108]
$C_2H_3 + C_3H_5 \rightarrow C_3H_6 + C_2H_2$	$8.00 \times 10^{-12}\,cm^3 \cdot s^{-1}$	[108]
$C_2H_3 + H_2 \rightarrow C_2H_4 + H$	$9.78 \times 10^{-20}\,cm^3 \cdot s^{-1}$	[105]
$C_2H_3 + H \rightarrow C_2H_2 + H_2$	$2.01 \times 10^{-11}\,cm^3 \cdot s^{-1}$	[106]
$C_2H_3 + H + CH_4 \rightarrow C_2H_4 + CH_4$	$2.02 \times 10^{-10}\,cm^3 \cdot s^{-1}$	[113]
	$8.26 \times 10^{-30}\,cm^6 \cdot s^{-1}$	b
$C_2H_2 + C_2H \rightarrow C_4H_2 + H$	$1.50 \times 10^{-10}\,cm^3 \cdot s^{-1}$	[88]
$C_2H_2 + H \rightarrow C_2H + H_2$	$6.12 \times 10^{-27}\,cm^3 \cdot s^{-1}$	[105]
$C_2H_2 + H + CH_4 \rightarrow C_2H_3 + CH_4$	$2.81 \times 10^{-31}\,cm^6 \cdot s^{-1}$	[106]
$C_2H + C_2H \rightarrow C_2H_2 + C_2$	$3.01 \times 10^{-12}\,cm^3 \cdot s^{-1}$	[105]
$C_2H + C_3H_8 \rightarrow C_2H_2 + C_3H_7$	$5.99 \times 10^{-12}\,cm^3 \cdot s^{-1}$	[107]
$C_2H + C_3H_7 \rightarrow C_3H_6 + C_2H_2$	$1.00 \times 10^{-11}\,cm^3 \cdot s^{-1}$	[107]
$C_2H + C_3H_6 \rightarrow C_3H_5 + C_2H_2$	$5.99 \times 10^{-12}\,cm^3 \cdot s^{-1}$	[108]

DOI: 10.1002/ppap.201100027

Table A.3. (Continued)

$C_2H + H_2 \rightarrow C_2H_2 + H$	$1.52 \times 10^{-13}\,cm^3 \cdot s^{-1}$	[105]
$C_2H + H \rightarrow C_2 + H_2$	$1.66 \times 10^{-31}\,cm^3 \cdot s^{-1}$	[105]
$C_2H + H + CH_4 \rightarrow C_2H_2 + CH_4$	$2.31 \times 10^{-10}\,cm^3 \cdot s^{-1}$	[113]
	$9.44 \times 10^{-30}\,cm^6 \cdot s^{-1}$	b
$C_3H_8 + C_3H_5 \rightarrow C_3H_6 + C_3H_7$	$2.02 \times 10^{-28}\,cm^3 \cdot s^{-1}$	[108]
$C_3H_8 + H \rightarrow C_3H_7 + H_2$	$5.15 \times 10^{-17}\,cm^3 \cdot s^{-1}$	[107]
$C_3H_7 + C_3H_7 \rightarrow C_3H_6 + C_3H_8$	$2.81 \times 10^{-12}\,cm^3 \cdot s^{-1}$	[107]
$C_3H_7 + C_3H_6 \rightarrow C_3H_5 + C_3H_8$	$2.53 \times 10^{-20}\,cm^3 \cdot s^{-1}$	[108]
$C_3H_7 + C_3H_5 \rightarrow C_3H_6 + C_3H_6$	$3.00 \times 10^{-12}\,cm^3 \cdot s^{-1}$	[108]
$C_3H_7 + H_2 \rightarrow C_3H_8 + H$	$7.12 \times 10^{-21}\,cm^3 \cdot s^{-1}$	[107]
$C_3H_7 + H \rightarrow C_3H_6 + H_2$	$3.01 \times 10^{-12}\,cm^3 \cdot s^{-1}$	[107]
$C_3H_7 + H + CH_4 \rightarrow C_3H_8 + CH_4$	$9.68 \times 10^{-11}\,cm^3 \cdot s^{-1}$	[113]
	$3.96 \times 10^{-30}\,cm^6 \cdot s^{-1}$	b
$C_3H_6 + H \rightarrow C_3H_5 + H_2$	$6.94 \times 10^{-15}\,cm^3 \cdot s^{-1}$	[108]
$C_3H_6 + H + CH_4 \rightarrow C_3H_7 + CH_4$	$9.26 \times 10^{-14}\,cm^3 \cdot s^{-1}$	[108]
	$3.79 \times 10^{-33}\,cm^6 \cdot s^{-1}$	b
$C_3H_5 + H_2 \rightarrow C_3H_6 + H$	$2.05 \times 10^{-27}\,cm^3 \cdot s^{-1}$	[108]
$C_3H_5 + H + CH_4 \rightarrow C_3H_6 + CH_4$	$3.26 \times 10^{-10}\,cm^3 \cdot s^{-1}$	[114]
	$1.33 \times 10^{-29}\,cm^6 \cdot s^{-1}$	b
$H + H + CH_4 \rightarrow H_2 + CH_4$	$6.00 \times 10^{-33}\,cm^6 \cdot s^{-1}$	[106]

Table A.4. Ion–neutral reactions included in the model, as well as the corresponding rate coefficients and the references where these data were adopted from.

$CH_5^+ + CH_2 \rightarrow CH_3^+ + CH_4$	$9.60 \times 10^{-10}\,cm^3 \cdot s^{-1}$	[115]
$CH_5^+ + CH \rightarrow CH_2^+ + CH_4$	$6.90 \times 10^{-10}\,cm^3 \cdot s^{-1}$	[115]
$CH_5^+ + C \rightarrow CH^+ + CH_4$	$1.20 \times 10^{-09}\,cm^3 \cdot s^{-1}$	[115]
$CH_5^+ + C_2H_6 \rightarrow C_2H_5^+ + H_2 + CH_4$	$2.25 \times 10^{-10}\,cm^3 \cdot s^{-1}$	[116]
$CH_5^+ + C_2H_4 \rightarrow C_2H_5^+ + CH_4$	$1.50 \times 10^{-09}\,cm^3 \cdot s^{-1}$	[115]
$CH_5^+ + C_2H_2 \rightarrow C_2H_3^+ + CH_4$	$1.60 \times 10^{-09}\,cm^3 \cdot s^{-1}$	[115]
$CH_5^+ + C_2H \rightarrow C_2H_2^+ + CH_4$	$9.00 \times 10^{-10}\,cm^3 \cdot s^{-1}$	[115]
$CH_5^+ + C_2 \rightarrow C_2H^+ + CH_4$	$9.50 \times 10^{-10}\,cm^3 \cdot s^{-1}$	[115]
$CH_5^+ + H \rightarrow CH_4^+ + H_2$	$1.50 \times 10^{-10}\,cm^3 \cdot s^{-1}$	[115]
$CH_4^+ + CH_4 \rightarrow CH_5^+ + CH_3$	$1.50 \times 10^{-09}\,cm^3 \cdot s^{-1}$	[115]
$CH_4^+ + C_2H_6 \rightarrow C_2H_4^+ + CH_4 + H_2$	$1.91 \times 10^{-09}\,cm^3 \cdot s^{-1}$	[116]
$CH_4^+ + C_2H_4 \rightarrow C_2H_5^+ + CH_3$	$4.23 \times 10^{-10}\,cm^3 \cdot s^{-1}$	[115]
$CH_4^+ + C_2H_4 \rightarrow C_2H_4^+ + CH_4$	$1.38 \times 10^{-09}\,cm^3 \cdot s^{-1}$	[115]
$CH_4^+ + C_2H_2 \rightarrow C_2H_3^+ + CH_3$	$1.23 \times 10^{-09}\,cm^3 \cdot s^{-1}$	[115]
$CH_4^+ + C_2H_2 \rightarrow C_2H_2^+ + CH_4$	$1.13 \times 10^{-09}\,cm^3 \cdot s^{-1}$	[115]
$CH_4^+ + H_2 \rightarrow CH_5^+ + H$	$3.30 \times 10^{-11}\,cm^3 \cdot s^{-1}$	[115]
$CH_4^+ + H \rightarrow CH_3^+ + H_2$	$1.00 \times 10^{-11}\,cm^3 \cdot s^{-1}$	[115]
$CH_3^+ + CH_4 \rightarrow CH_4^+ + CH_3$	$1.36 \times 10^{-10}\,cm^3 \cdot s^{-1}$	[117]
$CH_3^+ + CH_4 \rightarrow C_2H_5^+ + H_2$	$1.20 \times 10^{-09}\,cm^3 \cdot s^{-1}$	[115]
$CH_3^+ + CH_2 \rightarrow C_2H_3^+ + H_2$	$9.90 \times 10^{-10}\,cm^3 \cdot s^{-1}$	[115]

Table A.4. (Continued)

$CH_3^+ + CH \rightarrow C_2H_2^+ + H_2$	$7.10 \times 10^{-10}\,cm^3 \cdot s^{-1}$	[115]
$CH_3^+ + C \rightarrow C_2H^+ + H_2$	$1.20 \times 10^{-09}\,cm^3 \cdot s^{-1}$	[115]
$CH_3^+ + C_2H_6 \rightarrow C_2H_5^+ + CH_4$	$1.48 \times 10^{-09}\,cm^3 \cdot s^{-1}$	[115]
$CH_3^+ + C_2H_4 \rightarrow C_2H_3^+ + CH_4$	$3.50 \times 10^{-10}\,cm^3 \cdot s^{-1}$	[115]
$CH_3^+ + C_2H_3 \rightarrow C_2H_3^+ + CH_3$	$3.00 \times 10^{-10}\,cm^3 \cdot s^{-1}$	[115]
$CH_2^+ + CH_4 \rightarrow CH_3^+ + CH_3$	$1.38 \times 10^{-10}\,cm^3 \cdot s^{-1}$	[39]
$CH_2^+ + CH_4 \rightarrow C_2H_5^+ + H$	$3.60 \times 10^{-10}\,cm^3 \cdot s^{-1}$	[115]
$CH_2^+ + CH_4 \rightarrow C_2H_4^+ + H_2$	$8.40 \times 10^{-10}\,cm^3 \cdot s^{-1}$	[115]
$CH_2^+ + CH_4 \rightarrow C_2H_3^+ + H_2 + H$	$2.31 \times 10^{-10}\,cm^3 \cdot s^{-1}$	[39]
$CH_2^+ + CH_4 \rightarrow C_2H_2^+ + 2H_2$	$3.97 \times 10^{-10}\,cm^3 \cdot s^{-1}$	[39]
$CH_2^+ + C \rightarrow C_2H^+ + H$	$1.20 \times 10^{-09}\,cm^3 \cdot s^{-1}$	[115]
$CH_2^+ + H_2 \rightarrow CH_3^+ + H$	$1.60 \times 10^{-09}\,cm^3 \cdot s^{-1}$	[115]
$CH^+ + CH_4 \rightarrow C_2H_4^+ + H$	$6.50 \times 10^{-11}\,cm^3 \cdot s^{-1}$	[115]
$CH^+ + CH_4 \rightarrow C_2H_3^+ + H_2$	$1.09 \times 10^{-09}\,cm^3 \cdot s^{-1}$	[115]
$CH^+ + CH_4 \rightarrow C_2H_2^+ + H_2 + H$	$1.43 \times 10^{-10}\,cm^3 \cdot s^{-1}$	[115]
$CH^+ + CH_2 \rightarrow C_2H^+ + H_2$	$1.00 \times 10^{-09}\,cm^3 \cdot s^{-1}$	[115]
$CH^+ + CH \rightarrow C_2^+ + H_2$	$7.40 \times 10^{-10}\,cm^3 \cdot s^{-1}$	[115]
$CH^+ + C \rightarrow C_2^+ + H$	$1.20 \times 10^{-09}\,cm^3 \cdot s^{-1}$	[115]
$CH^+ + H_2 \rightarrow CH_2^+ + H$	$1.20 \times 10^{-09}\,cm^3 \cdot s^{-1}$	[115]
$CH^+ + H \rightarrow C^+ + H_2$	$7.50 \times 10^{-10}\,cm^3 \cdot s^{-1}$	[115]
$C^+ + CH_4 \rightarrow C_2H_3^+ + H$	$1.10 \times 10^{-09}\,cm^3 \cdot s^{-1}$	[115]
$C^+ + CH_4 \rightarrow C_2H_2^+ + H_2$	$4.00 \times 10^{-10}\,cm^3 \cdot s^{-1}$	[115]
$C^+ + CH_3 \rightarrow C_2H_2^+ + H$	$1.30 \times 10^{-09}\,cm^3 \cdot s^{-1}$	[115]
$C^+ + CH_3 \rightarrow C_2H^+ + H_2$	$1.00 \times 10^{-09}\,cm^3 \cdot s^{-1}$	[115]
$C^+ + CH_2 \rightarrow CH_2^+ + C$	$5.20 \times 10^{-10}\,cm^3 \cdot s^{-1}$	[115]
$C^+ + CH_2 \rightarrow C_2H^+ + H$	$5.20 \times 10^{-10}\,cm^3 \cdot s^{-1}$	[115]
$C^+ + CH \rightarrow CH^+ + C$	$3.80 \times 10^{-10}\,cm^3 \cdot s^{-1}$	[115]
$C^+ + CH \rightarrow C_2^+ + H$	$3.80 \times 10^{-10}\,cm^3 \cdot s^{-1}$	[115]
$C^+ + C_2H_6 \rightarrow C_2H_5^+ + CH$	$2.31 \times 10^{-10}\,cm^3 \cdot s^{-1}$	[115]
$C^+ + C_2H_6 \rightarrow C_2H_4^+ + CH_2$	$1.16 \times 10^{-10}\,cm^3 \cdot s^{-1}$	[115]
$C^+ + C_2H_6 \rightarrow C_2H_3^+ + CH_3$	$4.95 \times 10^{-10}\,cm^3 \cdot s^{-1}$	[115]
$C^+ + C_2H_6 \rightarrow C_2H_2^+ + CH_4$	$8.25 \times 10^{-11}\,cm^3 \cdot s^{-1}$	[115]
$C^+ + C_2H_5 \rightarrow C_2H_5^+ + C$	$5.00 \times 10^{-10}\,cm^3 \cdot s^{-1}$	[115]
$C^+ + C_2H_4 \rightarrow C_2H_4^+ + C$	$1.70 \times 10^{-11}\,cm^3 \cdot s^{-1}$	[115]
$C^+ + C_2H_4 \rightarrow C_2H_3^+ + CH$	$8.50 \times 10^{-11}\,cm^3 \cdot s^{-1}$	[115]
$C_2H_6^+ + C_2H_4 \rightarrow C_2H_4^+ + C_2H_6$	$1.15 \times 10^{-09}\,cm^3 \cdot s^{-1}$	[115]
$C_2H_6^+ + C_2H_2 \rightarrow C_2H_5^+ + C_2H_3$	$2.47 \times 10^{-10}\,cm^3 \cdot s^{-1}$	[115]
$C_2H_6^+ + H \rightarrow C_2H_5^+ + H_2$	$1.00 \times 10^{-10}\,cm^3 \cdot s^{-1}$	[115]
$C_2H_5^+ + H \rightarrow C_2H_4^+ + H_2$	$1.00 \times 10^{-11}\,cm^3 \cdot s^{-1}$	[115]
$C_2H_4^+ + C_2H_3 \rightarrow C_2H_5^+ + C_2H_2$	$5.00 \times 10^{-10}\,cm^3 \cdot s^{-1}$	[115]
$C_2H_4^+ + C_2H_3 \rightarrow C_2H_3^+ + C_2H_4$	$5.00 \times 10^{-10}\,cm^3 \cdot s^{-1}$	[115]
$C_2H_4^+ + H \rightarrow C_2H_3^+ + H_2$	$3.00 \times 10^{-10}\,cm^3 \cdot s^{-1}$	[115]
$C_2H_3^+ + C_2H_6 \rightarrow C_2H_5^+ + C_2H_4$	$2.91 \times 10^{-10}\,cm^3 \cdot s^{-1}$	[115]

DOI: 10.1002/ppap.201100027

Table A.4. (Continued)

$C_2H_3^+ + C_2H_4 \rightarrow C_2H_5^+ + C_2H_2$	$8.90 \times 10^{-10}\,cm^3 \cdot s^{-1}$	[115]
$C_2H_3^+ + C_2H_3 \rightarrow C_2H_5^+ + C_2H$	$5.00 \times 10^{-10}\,cm^3 \cdot s^{-1}$	[115]
$C_2H_3^+ + C_2H \rightarrow C_2H_2^+ + C_2H_2$	$3.30 \times 10^{-10}\,cm^3 \cdot s^{-1}$	[115]
$C_2H_3^+ + H \rightarrow C_2H_2^+ + H_2$	$6.80 \times 10^{-11}\,cm^3 \cdot s^{-1}$	[115]
$C_2H_2^+ + CH_4 \rightarrow C_2H_3^+ + CH_3$	$4.10 \times 10^{-09}\,cm^3 \cdot s^{-1}$	[39]
$C_2H_2^+ + C_2H_6 \rightarrow C_2H_5^+ + C_2H_3$	$1.31 \times 10^{-10}\,cm^3 \cdot s^{-1}$	[116]
$C_2H_2^+ + C_2H_6 \rightarrow C_2H_4^+ + C_2H_4$	$2.48 \times 10^{-10}\,cm^3 \cdot s^{-1}$	[115]
$C_2H_2^+ + C_2H_4 \rightarrow C_2H_4^+ + C_2H_2$	$4.14 \times 10^{-10}\,cm^3 \cdot s^{-1}$	[115]
$C_2H_2^+ + C_2H_3 \rightarrow C_2H_3^+ + C_2H_2$	$3.30 \times 10^{-10}\,cm^3 \cdot s^{-1}$	[115]
$C_2H_2^+ + H_2 \rightarrow C_2H_3^+ + H$	$1.00 \times 10^{-11}\,cm^3 \cdot s^{-1}$	[115]
$C_2H^+ + CH_4 \rightarrow C_2H_2^+ + CH_3$	$3.74 \times 10^{-10}\,cm^3 \cdot s^{-1}$	[115]
$C_2H^+ + CH_2 \rightarrow CH_3^+ + C_2$	$4.40 \times 10^{-10}\,cm^3 \cdot s^{-1}$	[115]
$C_2H^+ + CH \rightarrow CH_2^+ + C_2$	$3.20 \times 10^{-10}\,cm^3 \cdot s^{-1}$	[115]
$C_2H^+ + H_2 \rightarrow C_2H_2^+ + H$	$1.10 \times 10^{-09}\,cm^3 \cdot s^{-1}$	[115]
$C_2^+ + CH_4 \rightarrow C_2H_2^+ + CH_2$	$1.82 \times 10^{-10}\,cm^3 \cdot s^{-1}$	[115]
$C_2^+ + CH_4 \rightarrow C_2H^+ + CH_3$	$2.38 \times 10^{-10}\,cm^3 \cdot s^{-1}$	[115]
$C_2^+ + CH_2 \rightarrow CH_2^+ + C_2$	$4.50 \times 10^{-10}\,cm^3 \cdot s^{-1}$	[115]
$C_2^+ + CH \rightarrow CH^+ + C_2$	$3.20 \times 10^{-10}\,cm^3 \cdot s^{-1}$	[115]
$C_2^+ + C \rightarrow C^+ + C_2$	$1.10 \times 10^{-10}\,cm^3 \cdot s^{-1}$	[115]
$C_2^+ + H_2 \rightarrow C_2H^+ + H$	$1.10 \times 10^{-09}\,cm^3 \cdot s^{-1}$	[115]
$H_3^+ + CH_4 \rightarrow CH_5^+ + H_2$	$2.40 \times 10^{-09}\,cm^3 \cdot s^{-1}$	[115]
$H_3^+ + CH_3 \rightarrow CH_4^+ + H_2$	$2.10 \times 10^{-09}\,cm^3 \cdot s^{-1}$	[115]
$H_3^+ + CH_2 \rightarrow CH_3^+ + H_2$	$1.70 \times 10^{-09}\,cm^3 \cdot s^{-1}$	[115]
$H_3^+ + CH \rightarrow CH_2^+ + H_2$	$1.20 \times 10^{-09}\,cm^3 \cdot s^{-1}$	[115]
$H_3^+ + C \rightarrow CH^+ + H_2$	$2.00 \times 10^{-09}\,cm^3 \cdot s^{-1}$	[115]
$H_3^+ + C_2H_6 \rightarrow C_2H_5^+ + 2H_2$	$2.40 \times 10^{-09}\,cm^3 \cdot s^{-1}$	[115]
$H_3^+ + C_2H_5 \rightarrow C_2H_6^+ + H_2$	$1.40 \times 10^{-09}\,cm^3 \cdot s^{-1}$	[115]
$H_3^+ + C_2H_4 \rightarrow C_2H_5^+ + H_2$	$1.15 \times 10^{-09}\,cm^3 \cdot s^{-1}$	[115]
$H_3^+ + C_2H_4 \rightarrow C_2H_3^+ + 2H_2$	$1.15 \times 10^{-09}\,cm^3 \cdot s^{-1}$	[115]
$H_3^+ + C_2H_3 \rightarrow C_2H_4^+ + H_2$	$2.00 \times 10^{-09}\,cm^3 \cdot s^{-1}$	[115]
$H_3^+ + C_2H_2 \rightarrow C_2H_3^+ + H_2$	$3.50 \times 10^{-09}\,cm^3 \cdot s^{-1}$	[115]
$H_3^+ + C_2H \rightarrow C_2H_2^+ + H_2$	$1.70 \times 10^{-09}\,cm^3 \cdot s^{-1}$	[115]
$H_3^+ + C_2 \rightarrow C_2H^+ + H_2$	$1.80 \times 10^{-09}\,cm^3 \cdot s^{-1}$	[115]
$H_2^+ + CH_4 \rightarrow CH_5^+ + H$	$1.14 \times 10^{-10}\,cm^3 \cdot s^{-1}$	[115]
$H_2^+ + CH_4 \rightarrow CH_4^+ + H_2$	$1.40 \times 10^{-09}\,cm^3 \cdot s^{-1}$	[115]
$H_2^+ + CH_4 \rightarrow CH_3^+ + H_2 + H$	$2.30 \times 10^{-09}\,cm^3 \cdot s^{-1}$	[115]
$H_2^+ + CH_2 \rightarrow CH_3^+ + H$	$1.00 \times 10^{-09}\,cm^3 \cdot s^{-1}$	[115]
$H_2^+ + CH_2 \rightarrow CH_2^+ + H_2$	$1.00 \times 10^{-09}\,cm^3 \cdot s^{-1}$	[115]
$H_2^+ + CH \rightarrow CH_2^+ + H$	$7.10 \times 10^{-10}\,cm^3 \cdot s^{-1}$	[115]
$H_2^+ + CH \rightarrow CH^+ + H_2$	$7.10 \times 10^{-10}\,cm^3 \cdot s^{-1}$	[115]
$H_2^+ + C \rightarrow CH^+ + H$	$2.40 \times 10^{-09}\,cm^3 \cdot s^{-1}$	[115]
$H_2^+ + C_2H_6 \rightarrow C_2H_6^+ + H_2$	$2.94 \times 10^{-10}\,cm^3 \cdot s^{-1}$	[115]
$H_2^+ + C_2H_6 \rightarrow C_2H_5^+ + H_2 + H$	$1.37 \times 10^{-09}\,cm^3 \cdot s^{-1}$	[115]

Table A.4. (Continued)

$H_2^+ + C_2H_6 \rightarrow C_2H_4^+ + 2H_2$	$2.35 \times 10^{-09}\,cm^3 \cdot s^{-1}$	[115]
$H_2^+ + C_2H_6 \rightarrow C_2H_3^+ + 2H_2 + H$	$6.86 \times 10^{-10}\,cm^3 \cdot s^{-1}$	[116]
$H_2^+ + C_2H_6 \rightarrow C_2H_2^+ + 3H_2$	$1.96 \times 10^{-10}\,cm^3 \cdot s^{-1}$	[116]
$H_2^+ + C_2H_4 \rightarrow C_2H_4^+ + H_2$	$2.21 \times 10^{-09}\,cm^3 \cdot s^{-1}$	[115]
$H_2^+ + C_2H_4 \rightarrow C_2H_3^+ + H_2 + H$	$1.81 \times 10^{-09}\,cm^3 \cdot s^{-1}$	[115]
$H_2^+ + C_2H_4 \rightarrow C_2H_2^+ + 2H_2$	$8.82 \times 10^{-10}\,cm^3 \cdot s^{-1}$	[115]
$H_2^+ + C_2H_2 \rightarrow C_2H_3^+ + H$	$4.80 \times 10^{-10}\,cm^3 \cdot s^{-1}$	[115]
$H_2^+ + C_2H_2 \rightarrow C_2H_2^+ + H_2$	$4.82 \times 10^{-09}\,cm^3 \cdot s^{-1}$	[115]
$H_2^+ + C_2H \rightarrow C_2H_2^+ + H$	$1.00 \times 10^{-09}\,cm^3 \cdot s^{-1}$	[115]
$H_2^+ + C_2H \rightarrow C_2H^+ + H_2$	$1.00 \times 10^{-09}\,cm^3 \cdot s^{-1}$	[115]
$H_2^+ + C_2 \rightarrow C_2H^+ + H$	$1.10 \times 10^{-09}\,cm^3 \cdot s^{-1}$	[115]
$H_2^+ + C_2 \rightarrow C_2^+ + H_2$	$1.10 \times 10^{-09}\,cm^3 \cdot s^{-1}$	[115]
$H_2^+ + H_2 \rightarrow H_3^+ + H$	$2.08 \times 10^{-09}\,cm^3 \cdot s^{-1}$	[115]
$H_2^+ + H \rightarrow H^+ + H_2$	$6.40 \times 10^{-10}\,cm^3 \cdot s^{-1}$	[115]
$H^+ + CH_4 \rightarrow CH_4^+ + H$	$1.50 \times 10^{-09}\,cm^3 \cdot s^{-1}$	[115]
$H^+ + CH_4 \rightarrow CH_3^+ + H_2$	$2.30 \times 10^{-09}\,cm^3 \cdot s^{-1}$	[115]
$H^+ + CH_3 \rightarrow CH_3^+ + H$	$3.40 \times 10^{-09}\,cm^3 \cdot s^{-1}$	[115]
$H^+ + CH_2 \rightarrow CH_2^+ + H$	$1.40 \times 10^{-09}\,cm^3 \cdot s^{-1}$	[115]
$H^+ + CH_2 \rightarrow CH^+ + H_2$	$1.40 \times 10^{-09}\,cm^3 \cdot s^{-1}$	[115]
$H^+ + CH \rightarrow CH^+ + H$	$1.90 \times 10^{-09}\,cm^3 \cdot s^{-1}$	[115]
$H^+ + C_2H_6 \rightarrow C_2H_5^+ + H_2$	$1.30 \times 10^{-09}\,cm^3 \cdot s^{-1}$	[115]
$H^+ + C_2H_6 \rightarrow C_2H_4^+ + H_2 + H$	$1.40 \times 10^{-09}\,cm^3 \cdot s^{-1}$	[115]
$H^+ + C_2H_6 \rightarrow C_2H_3^+ + 2H_2$	$2.80 \times 10^{-09}\,cm^3 \cdot s^{-1}$	[115]
$H^+ + C_2H_5 \rightarrow C_2H_4^+ + H_2$	$1.65 \times 10^{-09}\,cm^3 \cdot s^{-1}$	[115]
$H^+ + C_2H_5 \rightarrow C_2H_3^+ + H_2 + H$	$3.06 \times 10^{-09}\,cm^3 \cdot s^{-1}$	[115]
$H^+ + C_2H_4 \rightarrow C_2H_4^+ + H$	$1.00 \times 10^{-09}\,cm^3 \cdot s^{-1}$	[115]
$H^+ + C_2H_4 \rightarrow C_2H_3^+ + H_2$	$3.00 \times 10^{-09}\,cm^3 \cdot s^{-1}$	[115]
$H^+ + C_2H_4 \rightarrow C_2H_2^+ + H_2 + H$	$1.00 \times 10^{-09}\,cm^3 \cdot s^{-1}$	[115]
$H^+ + C_2H_3 \rightarrow C_2H_3^+ + H$	$2.00 \times 10^{-09}\,cm^3 \cdot s^{-1}$	[115]
$H^+ + C_2H_3 \rightarrow C_2H_2^+ + H_2$	$2.00 \times 10^{-09}\,cm^3 \cdot s^{-1}$	[115]
$H^+ + C_2H_2 \rightarrow C_2H_2^+ + H$	$5.40 \times 10^{-10}\,cm^3 \cdot s^{-1}$	[115]
$H^+ + C_2H \rightarrow C_2H^+ + H$	$1.50 \times 10^{-09}\,cm^3 \cdot s^{-1}$	[115]
$H^+ + C_2H \rightarrow C_2^+ + H_2$	$1.50 \times 10^{-09}\,cm^3 \cdot s^{-1}$	[115]
$H^+ + C_2 \rightarrow C_2^+ + H$	$3.10 \times 10^{-09}\,cm^3 \cdot s^{-1}$	[115]

Acknowledgements: Funding of this work by the Instituut voor aanmoediging van innovatie door Wetenschap en Technologie in Vlaanderen (IWT) and the calculation support of the core facility CALCUA, provided by the University of Antwerp, are gratefully acknowledged.

Received: February 3, 2011; Revised: May 30, 2011; Accepted: June 8, 2011; DOI: 10.1002/ppap.201100027

Keywords: atmospheric pressure; dielectric barrier discharges (DBD); gas conversion; methane; modeling

[1] International Energy Agency, *World Energy Outlook, 2008*, Paris 2008.
[2] World Energy Council, *Survey of Energy Resources, 2007*, London 2007.
[3] Intergovernmental Panel on Climate Change, *Climate Change 2007: Synthesis Report*, Geneva 2007.

[4] J. H. Lunsford, *Catal. Today* **2000**, *63*, 165.
[5] F. M. Aghamir, N. S. Matin, A. H. Jalili, M. H. Esfarayeni, M. A. Khodagholi, R. Ahmadi, *Plasma Sources Sci. Technol.* **2004**, *13*, 707.
[6] J. J. Zou, Y. P. Zhang, C. J. Liu, Y. Li, B. Eliasson, *Plasma Chem. Plasma Process.* **2003**, *23*, 69.
[7] J. F. Roth, *Appl. Catal. A Gen.* **1994**, *113*, 131.
[8] B. Eliasson, U. Kogelschatz, *IEEE Trans. Plasma Sci.* **1991**, *19*, 309.
[9] V. I. Gibalov, G. J. Pietsch, *J. Phys. D, Appl. Phys.* **2000**, *33*, 2618.
[10] H. Conrads, M. Schmidt, *Plasma Sources Sci. Technol.* **2000**, *9*, 441.
[11] U. Kogelschatz, *IEEE Trans. Plasma Sci.* **2002**, *30*, 1400.
[12] A. Bogaerts, E. Neyts, R. Gijbels, J. van der Mullen, *Spectrochim. Acta B* **2002**, *57*, 609.
[13] U. Kogelschatz, *Plasma Chem. Plasma Process.* **2003**, *23*, 1.
[14] U. Kogelschatz, B. Eliasson, W. Egli, *Pure Appl. Chem.* **1999**, *71*, 1819.
[15] H. H. Kim, *Plasma Process. Polym.* **2004**, *1*, 91.
[16] J. S. Chang, *Plasma Sources Sci. Technol.* **2008**, *17*, 045004.
[17] M. B. Chang, J. H. Balbach, M. J. Rood, M. J. Kushner, *J. Appl. Phys.* **1991**, *69*, 4409.
[18] M. B. Chang, M. J. Kushner, M. J. Rood, *Plasma Chem. Plasma Process.* **1992**, *12*, 565.
[19] M. B. Chang, M. J. Kushner, M. J. Rood, *Environ. Sci. Technol.* **1992**, *26*, 777.
[20] S. K. Dhali, I. Sardja, *J. Appl. Phys.* **1991**, *69*, 6319.
[21] L. M. Zhou, B. Xue, U. Kogelschatz, B. Eliasson, *Energy Fuel* **1998**, *12*, 1191.
[22] L. M. Zhou, B. Xue, U. Kogelschatz, B. Eliasson, *Plasma Chem. Plasma Process.* **1998**, *18*, 375.
[23] B. Eliasson, C. J. Liu, U. Kogelschatz, *Ind. Eng. Chem. Res.* **2000**, *39*, 1221.
[24] D. W. Larkin, L. L. Lobban, R. G. Mallinson, *Catal. Today* **2001**, *71*, 199.
[25] C. J. Liu, B. Eliasson, B. Z. Xue, Y. Li, Y. Q. Wang, *React. Kinet. Catal. Lett.* **2001**, *74*, 71.
[26] C. J. Liu, B. Z. Xue, B. Eliasson, F. He, Y. Li, G. H. Xu, *Plasma Chem. Plasma Process.* **2001**, *21*, 301.
[27] T. Jiang, Y. Li, C. J. Liu, G. H. Xu, B. Eliasson, B. Z. Xue, *Catal. Today* **2002**, *72*, 229.
[28] K. Zhang, B. Eliasson, U. Kogelschatz, *Ind. Eng. Chem. Res.* **2002**, *41*, 1462.
[29] Y. Yang, *Plasma Chem. Plasma Process.* **2003**, *23*, 283.
[30] A. A. Khassin, B. L. Pietruszka, M. Heintze, V. N. Parmon, *React. Kinet. Catal. Lett.* **2004**, *82*, 111.
[31] B. Pietruszka, K. Anklam, M. Heintze, *Appl. Catal. A Gen.* **2004**, *261*, 19.
[32] B. Pietruszka, M. Heintze, *Catal. Today* **2004**, *90*, 151.
[33] H. K. Song, J. W. Choi, S. H. Yue, H. Lee, B. K. Na, *Catal. Today* **2004**, *89*, 27.
[34] I. Istadi, N. A. S. Amin, *Fuel* **2006**, *85*, 577.
[35] S. S. Kim, H. Lee, J. W. Choi, B. K. Na, H. K. Song, *Catal. Commun.* **2007**, *8*, 1438.
[36] A. Indarto, *J. Chin. Inst. Chem. Eng.* **2008**, *39*, 23.
[37] N. S. Matin, H. A. Savadkoohi, S. Y. Feizabadi, *Plasma Chem. Plasma Process.* **2008**, *28*, 189.
[38] G. Scarduelli, G. Guella, D. Ascenzi, P. Tosi, *Plasma Process. Polym.* **2011**, *8*, 25.
[39] K. Tachibana, M. Nishida, H. Harima, Y. Urano, *J. Phys. D, Appl. Phys.* **1984**, *17*, 1727.
[40] E. Gogolides, C. Buteau, A. Rhallabi, G. Turban, *J. Phys. D, Appl. Phys.* **1994**, *27*, 818.
[41] E. Gogolides, D. Mary, A. Rhallabi, G. Turban, *Jpn. J. Appl. Phys. 1* **1995**, *34*, 261.
[42] M. Masi, C. Cavallotti, S. Carra, *Chem. Eng. Sci.* **1998**, *53*, 3875.
[43] W. Y. Fan, P. F. Knewstubb, M. Kaning, L. Mechold, J. Ropcke, P. B. Davies, *J. Phys. Chem. A* **1999**, *103*, 4118.
[44] D. Herrebout, A. Bogaerts, M. Yan, R. Gijbels, W. Goedheer, A. Vanhulsel, *J. Appl. Phys.* **2002**, *92*, 2290.
[45] M. Kraus, W. Egli, K. Haffner, B. Eliasson, U. Kogelschatz, A. Wokaun, *Phys. Chem. Chem. Phys.* **2002**, *4*, 668.
[46] S. F. Yoon, K. H. Tan, Rusli, J. Ahn, *J. Appl. Phys.* **2002**, *91*, 40.
[47] D. Herrebout, A. Bogaerts, R. Gijbels, W. J. Goedheer, A. Vanhulsel, *IEEE Trans. Plasma Sci.* **2003**, *31*, 659.
[48] Y. Yang, *Plasma Chem. Plasma Process.* **2003**, *23*, 327.
[49] C. Q. Jiang, A. A. H. Mohamed, R. H. Stark, J. H. Yuan, K. H. Schoenbach, *IEEE Trans. Plasma Sci.* **2005**, *33*, 1416.
[50] T. Kovacs, R. T. Deam, *J. Phys. D, Appl. Phys.* **2006**, *39*, 2391.
[51] I. Istadi, N. A. S. Amin, *Chem. Eng. Sci.* **2007**, *62*, 6568.
[52] G. V. Naidis, *J. Phys. D, Appl. Phys.* **2007**, *40*, 4525.
[53] S. A. Nair, T. Nozaki, K. Okazaki, *Chem. Eng. J.* **2007**, *132*, 85.
[54] C. D. Pintassilgo, C. Jaoul, J. Loureiro, T. Belmonte, T. Czerwiec, *J. Phys. D, Appl. Phys.* **2007**, *40*, 3620.
[55] A. Agiral, C. Trionfetti, L. Lefferts, K. Seshan, J. G. E. Gardeniers, *Chem. Eng. Technol.* **2008**, *31*, 1116.
[56] A. Indarto, N. Coowanitwong, J.-W. Choi, H. Lee, H. K. Song, *Fuel Process. Technol.* **2008**, *89*, 214.
[57] J. Luche, O. Aubry, A. Khacef, J. M. Cormier, *Chem. Eng. J.* **2009**, *149*, 35.
[58] G. J. M. Hagelaar, Modeling of Microdischarges for Display Technology, *PhD Thesis*, Eindhoven University of Technology, **2000**.
[59] G. J. M. Hagelaar, G. M. W. Kroesen, U. van Slooten, H. Schreuders, *J. Appl. Phys.* **2000**, *88*, 2252.
[60] G. J. M. Hagelaar, G. M. W. Kroesen, *J. Comput. Phys.* **2000**, *159*, 1.
[61] G. J. M. Hagelaar, F. J. de Hoog, G. M. W. Kroesen, *Phys. Rev. E* **2000**, *62*, 1452.
[62] W. J. M. Brok, J. van Dijk, M. D. Bowden, J. J. A. M. van der Mullen, G. M. W. Kroesen, *J. Phys. D, Appl. Phys.* **2003**, *36*, 1967.
[63] W. J. M. Brok, M. F. Gendre, J. J. A. M. van der Mullen, *J. Phys. D, Appl. Phys.* **2007**, *40*, 156.
[64] W. J. M. Brok, M. F. Gendre, M. Haverlag, J. J. A. M. van der Mullen, *J. Phys. D, Appl. Phys.* **2007**, *40*, 3931.
[65] W. J. M. Brok, M. D. Bowden, J. van Dijk, J. J. A. M. van der Mullen, G. M. W. Kroesen, *J. Appl. Phys.* **2005**, *98*, 013302.
[66] E. Wagenaars, R. Brandenburg, W. J. M. Brok, M. D. Bowden, H. E. Wagner, *J. Phys. D, Appl. Phys.* **2006**, *39*, 700.
[67] T. Martens, A. Bogaerts, W. Brok, J. van Dijk, *Anal. Bioanal. Chem.* **2007**, *388*, 1583.
[68] T. Martens, A. Bogaerts, W. J. M. Brok, J. J. A. M. van der Mullen, *J. Anal. Atom. Spectrom.* **2007**, *22*, 1033.
[69] T. Martens, D. Mihailova, J. van Dijk, A. Bogaerts, *Anal. Chem.* **2009**, *81*, 9096.
[70] M. Meyyappan, J. P. Kreskovsky, *J. Appl. Phys.* **1990**, *68*, 1506.
[71] E. Gogolides, H. H. Sawin, *J. Appl. Phys.* **1992**, *72*, 3971.
[72] J. D. P. Passchier, W. J. Goedheer, *J. Appl. Phys.* **1993**, *74*, 3744.
[73] J. Meunier, P. Belenguer, J. P. Boeuf, *J. Appl. Phys.* **1995**, *78*, 731.
[74] C. Punset, J. P. Boeuf, L. C. Pitchford, *J. Appl. Phys.* **1998**, *83*, 1884.
[75] D. Mihailova, M. Grozeva, G. J. M. Hagelaar, J. van Dijk, W. J. M. Brok, J. J. A. M. van der Mullen, *J. Phys. D, Appl. Phys.* **2008**, *41*, 245202.

[76] G. E. Schneider, M. Zedan, *Numer. Heat Transf. A-Appl.* **1981**, *4*, 1.
[77] S. Paulussen, B. Verheyde, X. Tu, C. De Bie, T. Martens, D. Petrovic, A. Bogaerts, B. Sels, *Plasma Sources Sci. Technol.* **2010**, *19*, 034015.
[78] D. Herrebout, A. Bogaerts, M. Yan, R. Gijbels, W. Goedheer, E. Dekempeneer, *J. Appl. Phys.* **2001**, *90*, 570.
[79] T. Farouk, B. Farouk, A. Gutsol, A. Fridman, *J. Phys. D, Appl. Phys.* **2008**, *41*, 175202.
[80] W. L. Morgan, *Plasma Chem. Plasma Process.* **1992**, *12*, 477.
[81] R. C. Reid, J. M. Prausnitz, B. E. Poling, *The Properties of Gases and Liquids*, 4th edition, McGraw-Hill Book Company, New York **1987**.
[82] R. A. Svehla, *Estimated Viscosities and Thermal Conductivities of Gases at High Temperatures*, National Aeronautics and Space Administration, Washington DC **1962**.
[83] E. W. Mcdaniel, E. A. Mason, *The Mobility and Diffusion of Ions in Gases*, John Wiley & Sons, New York **1973**.
[84] C. J. F. Böttcher, P. Bordewijk, *Theory of Electric Polarization*, 2nd edition, *Vol. 2*, Dielectrics in Time-Dependent Fields, Elsevier Scientific Publishing Company, Amsterdam **1978**, p. 332.
[85] G. J. M. Hagelaar, L. C. Pitchford, *Plasma Sources Sci. Technol.* **2005**, *14*, 722.
[86] W. Bohmeyer, D. Naujoks, A. Markin, I. Arkhipov, B. Koch, D. Schroder, G. Fussmann, *J. Nucl. Mater.* **2005**, *337–339*, 89.
[87] M. Eckert, E. Neyts, A. Bogaerts, *Chem. Vapor Depos.* **2008**, *14*, 213.
[88] D. L. Baulch, C. J. Cobos, R. A. Cox, P. Frank, G. Hayman, T. Just, J. A. Kerr, T. Murrells, M. J. Pilling, J. Troe, R. W. Walker, J. Warnatz, *J. Phys. Chem. Ref. Data* **1994**, *23*, 847.
[89] A. H. Laufer, E. P. Gardner, T. L. Kwok, Y. L. Yung, *Icarus* **1983**, *56*, 560.
[90] T. Martens, W. J. M. Brok, J. van Dijk, A. Bogaerts, *J. Phys. D, Appl. Phys.* **2009**, *42*, 122002.
[91] K. De Bleecker, A. Bogaerts, W. Goedheer, *Phys. Rev. E* **2006**, *73*, 026405.
[92] K. De Bleecker, A. Bogaerts, W. Goedheer, *Appl. Phys. Lett.* **2006**, *88*, 151501.
[93] M. Mao, J. Benedikt, A. Consoli, A. Bogaerts, *J. Phys. D, Appl. Phys.* **2008**, *41*, 225201.
[94] R. K. Janev, *Atomic and Molecular Processes in Fusion Edge Plasmas*, Plenum Press, New York **1995**.
[95] R. K. Janev, J. G. Wang, I. Murakami, T. Kato, *Cross Sections and Rate Coefficients for Electron-Impact Ionization of Hydrocarbon Molecules*, National Institute for Fusion Science (NIFS) of Japan, Toki, Gifu **2001**.
[96] R. K. Janev, D. Reiter, *Phys. Plasmas* **2002**, *9*, 4071.
[97] R. K. Janev, D. Reiter, *ChemInform* **2003**, *34*, DOI: 10.1002/chin.200325274.
[98] R. K. Janev, D. Reiter, *ChemInform* **2003**, *34*, DOI: 10.1002/chin.200337260.
[99] R. K. Janev, D. Reiter, *Phys. Plasmas* **2004**, *11*, 780.
[100] A. G. Engelhardt, A. V. Phelps, *Phys. Rev.* **1963**, *131*, 2115.
[101] S. Trajmar, D. F. Register, A. Chutjian, *Phys. Rep.* **1983**, *97*, 221.
[102] H. Tawara, T. Kato, *Atom. Data Nucl. Data* **1987**, *36*, 167.
[103] S. J. B. Corrigan, *J. Chem. Phys.* **1965**, *43*, 4381.
[104] A. I. Florescu-Mitchell, J. B. A. Mitchell, *Phys. Rep.* **2006**, *430*, 277.
[105] W. Tsang, R. F. Hampson, *J. Phys. Chem. Ref. Data* **1986**, *15*, 1087.
[106] D. L. Baulch, C. J. Cobos, R. A. Cox, C. Esser, P. Frank, T. Just, J. A. Kerr, M. J. Pilling, J. Troe, R. W. Walker, J. Warnatz, *J. Phys. Chem. Ref. Data* **1992**, *21*, 411.
[107] W. Tsang, *J. Phys. Chem. Ref. Data* **1988**, *17*, 887.
[108] W. Tsang, *J. Phys. Chem. Ref. Data* **1991**, *20*, 221.
[109] P. H. Stewart, C. W. Larson, D. M. Golden, *Combust. Flame* **1989**, *75*, 25.
[110] A. H. Laufer, A. Fahr, *Chem. Rev.* **2004**, *104*, 2813.
[111] L. B. Harding, R. Guadagnini, G. C. Schatz, *J. Phys. Chem.* **1993**, *97*, 5472.
[112] S. Y. Lin, H. Guo, *J. Phys. Chem. A* **2004**, *108*, 10066.
[113] L. B. Harding, Y. Georgievskii, S. J. Klippenstein, *J. Phys. Chem. A* **2005**, *109*, 4646.
[114] L. B. Harding, S. J. Klippenstein, Y. Georgievskii, *J. Phys. Chem. A* **2007**, *111*, 3789.
[115] J. Woodall, M. Agúndez, A. J. Markwick-Kemper, T. J. Millar, *Astron. Astrophys.* **2007**, *466*, 1197.
[116] Y. H. Kim, J. L. Fox, *Icarus* **1994**, *112*, 310.
[117] H. Tahara, K. Minami, A. Murai, T. Yasui, T. Yoshikawa, *Jpn. J. Appl. Phys. 1* **1995**, *34*, 1972.

DOI: 10.1002/ppap.201100027